Journal of Molecular Graphics and Modelling 77 (2017) 33–50

Contents lists available at ScienceDirect

Journal of Molecular Graphics and Modelling

journal homepage: www.elsevier.com/locate/JMGM

Crystal structures of nematode (parasitic *T. spiralis* and free living *C. elegans*), compared to mammalian, thymidylate synthases (TS). Molecular docking and molecular dynamics simulations in search for nematode-specific inhibitors of TS

Adam Jarmuła[a,*], Piotr Wilk[a,b], Piotr Maj[a], Jan Ludwiczak[a,c], Anna Dowierciał[a], Katarzyna Banaszak[d], Wojciech Rypniewski[d], Joanna Cieśla[a], Magdalena Dąbrowska[a], Tomasz Frączyk[a], Agnieszka K. Bronowska[e], Jakub Jakowiecki[f], Sławomir Filipek[f], Wojciech Rode[a]

[a] *Nencki Institute of Experimental Biology, Polish Academy of Sciences, Warszawa, Poland*
[b] *Macromolecular Crystallography (BESSY-MX), Berlin, Germany*
[c] *Centre of New Technologies, University of Warsaw, Warszawa, Poland*
[d] *Institute of Bioorganic Chemistry, Polish Academy of Sciences, Poznań, Poland*
[e] *Faculty of Chemistry, University of Heidelberg, Heidelberg, Germany*
[f] *Faculty of Chemistry, University of Warsaw, Warszawa, Poland*

ARTICLE INFO

Article history:
Received 16 June 2017
Received in revised form 5 August 2017
Accepted 7 August 2017
Available online 12 August 2017

Keywords:
Thymidylate synthase (TS)
Crystal structures
Molecular docking
Inhibitors of *Trichinella spiralis* TS

ABSTRACT

Three crystal structures are presented of nematode thymidylate synthases (TS), including *Caenorhabditis elegans* (*Ce*) enzyme without ligands and its ternary complex with dUMP and Raltitrexed, and binary complex of *Trichinella spiralis* (*Ts*) enzyme with dUMP. In search of differences potentially relevant for the development of species-specific inhibitors of the nematode enzyme, a comparison was made of the present *Ce* and *Ts* enzyme structures, as well as binary complex of *Ce* enzyme with dUMP, with the corresponding mammalian (human, mouse and rat) enzyme crystal structures. To complement the comparison, tCONCOORD computations were performed to evaluate dynamic behaviors of mammalian and nematode TS structures. Finally, comparative molecular docking combined with molecular dynamics and free energy of binding calculations were carried out to search for ligands showing selective affinity to *T. spiralis* TS. Despite an overall strong similarity in structure and dynamics of nematode vs mammalian TSs, a pool of ligands demonstrating predictively a strong and selective binding to *Ts*TS has been delimited. These compounds, the E63 family, locate in the dimerization interface of *Ts*TS where they exert species-specific interactions with certain non-conserved residues, including hydrogen bonds with Thr174 and hydrophobic contacts with Phe192, Cys191 and Tyr152. The E63 family of ligands opens the possibility of future development of selective inhibitors of *Ts*TS and effective agents against trichinellosis.

1. Introduction

Nematodes encompass numerous parasitic species, belonging to the most common infectious agents of humans, majority of infections taking place in the developing countries [1–3]. One example is *Trichinella spiralis*, causing a serious disease, trichinellosis, in both developing and developed countries [4,5]. Another nematode, *Caenorhabditis elegans* is a commonly used model organism, including in parasitological studies [6–8].

Thymidylate synthase (EC 2.1.1.45; TS), catalyzing the reductive methylation of deoxyuridine monophosphate (dUMP) by $N^{5,10}$-methylenetetrahydrofolate (meTHF) to generate thymidylate (dTMP) and dihydrofolate (DHF), is a key target for anticancer, antiviral, antifungal and antiprotozoan chemotherapy [9–15].

The present study relates to our earlier observation of high specific activity of TS present not only in *Trichinella spiralis* adult forms, but surprisingly (lack of cell proliferation) also in devel-

Abbreviations: TS, thymidylate synthase; *Ce*, *Caenorhabditis elegans*; *Ec*, *Escherichia coli*; *Lc*, *Lactobacillus casei*; *Ts*, *Trichinella spiralis*; DHFR, dihydrofolate reductase.

* Corresponding author.
E-mail address: a.jarmula@nencki.gov.pl (A. Jarmuła).

http://dx.doi.org/10.1016/j.jmgm.2017.08.008
1093-3263/

opmentally arrested muscle larvae [16–20]. Notably, we found similar phenomenon to take place in the development of the free living nematode *Caenorhabditis elegans* [18], whose developmentally arrested dauer larvae correspond to developmentally arrested infective larvae of parasitic nematodes [6], such as *T. spiralis* muscle larvae. An unusual cell cycle regulation, involving long term cell cycle arrest, is suggested to play a role in developmentally arrested *Trichinella* muscle larvae and *C. elegans* dauer larvae, resulting, among others, in high TS level (discussed in [16,18]). TS protein, present in developmentally arrested forms, is probably catalytically irrelevant (no DNA synthesis), but may play a regulatory role, as the enzyme shows certain non-catalytic activities, including capacity to bind mRNA (its own and some others) and inhibit translation, and is suspected to be engaged in regulation of several cellular genes [21], as well as to exert an oncogene-like activity [22]. Therefore, finding a possibility of selective interference with nematode TS catalytic/non-catalytic activities could provide both a therapeutic method and a means to study the physiological significance of the high expression of TS in nematodes' cells, particularly in their developmentally arrested forms.

Thymidylate synthase protein, and its active site in particular, belong to the most conservative [23–26]. Therefore, inhibitors designed as substrate/cofactor analogues are rather beyond hope as candidates for species-selective inhibitors of the pathogen *vs.* mammalian enzyme (*cf.* [16], for a comparison of interaction of several such analogues with the enzyme isolated from *T. spiralis* muscle larvae and regenerating rat liver). A promising way of solving such problems was developed in the line of work initiated by [27], who applied molecular docking to a *Lactobacillus casei* TS (*Lc*TS) target, and obtained several hits structurally distinct from previously known TS inhibitors. Sulisobenzon (capable of only weak TS inhibition), revealed an altered orientation of conserved Trp85 in the active site of the enzyme. Further cycles of virtual screening yielded stronger inhibitors like phenytoin, and the most potent group consisting of phenolphthalein (PTH) and its derivatives with either phthalide ring or phenyl rings modified. Following years brought several papers demonstrating inhibitors taking advantage of features that differ bacterial TS (most often *Lc*TS or *Escherichia coli* TS; *Ec*TS) from its human counterpart in order to gain selectivity towards the bacterial enzyme [28–41], with naphthalein derivative of PTH, α-156, being the first species-selective TS inhibitor affecting bacterial enzyme 40 times stronger than the human one [28] (called compound 4 in that paper).

Considering similar approach with respect to nematodes, it should be mentioned that until recently the only known metazoan TS 3D structures were those of human [42–52], rat [53] and mouse [54].

Another approach aimed at designing novel groups of TS inhibitors that could be used in a species-specific manner or help to tackle drug resistance in cancer chemotherapy [51,55] involves targeting the enzyme dimerization interface. Effective inhibition of the enzyme by targeting the interface is exemplified by a synthetic peptide corresponding to a segment of the dimerization interface of *Lc*TS (residues 201–220), shown to inhibit the enzyme's catalytic activity [56], as well as peptide inhibitors of human TS [51,57–61]. Differences in the amino acid sequence of the interface region of TSs of different specific origin can be exploited in designing species-specific inhibitors of *Toxoplasma gondii* TS-DHFR in the form of either peptides [62] or small molecules [63].

2. Materials and methods

2.1. Chemicals

Raltitrexed, 2′-deoxyuridylate (dUMP), $Al(OH)_3$, Tris, DTT, MgCl2, (NH4)2SO4, PEG 4000, PEG 5000 MME, PEG 3350, Bis-Tris, and sodium acetate were from Sigma-Aldrich (St. Louis, MO, USA), (6*RS*)-$N^{5,10}$-methylenetetrahydrofolate, calcium salt from Schircks Laboratories (Jona, Switzerland), Ni-NTA His-Bind Resin from Novagen (Madison, WI, USA), Pro-Q Diamond Phosphoprotein Gel Stain and SYPRO Ruby Protein Gel Stain from Thermo Fischer Scientific (Waltham, MA, USA) and Amicon Centricon centrifugal filter from Merck Millipore (Billerica, MA, USA).

2.2. TS preparation

T. spiralis TS coding region [17] was subcloned into pQE2 vector and expressed as a HisTag-containing protein in a JM109 *E. coli* strain. The HisTag-containing protein was purified on Ni-NTA His-Bind Resin (Novagen) according to the manufacturer's protocol. *C. elegans* TS was expressed and purified as described earlier [18]. With both TS proteins phosphatase inhibitors were present in all purification buffers as described earlier [64]. TS activity was monitored as previously described [16].

2.3. Separation of TS preparations into phosphorylated and non-phosphorylated fractions

This was done according to [65], using metal oxide/hydroxide affinity chromatography (MOAC) on $Al(OH)_3$ beads. With both *T. spiralis* and *C. elegans* enzymes the non-phosphorylated fractions were used for crystallization. Separation was inspected visually using Pro-Q Diamond Phosphoprotein Gel Stain and SYPRO Ruby Protein Gel Stain applied after SDS-PAGE as described earlier [66].

2.4. Crystallization and data collection

Each purified *T. spiralis* and *C. elegans* TS recombinant protein was dialyzed against 5 mM Tris HCl buffer, pH 7.5, containing 5 mM DTT, and concentrated using an Amicon Centricon centrifugal filter (cf. [67]). Crystals were grown by the vapor diffusion method in hanging drops at room temperature (*Ts*TS) or at 4 °C (*Ce*TS). With the *T. spiralis* enzyme, 3.5 μL of the protein solution and 2 μL of the corresponding well solution (Table 1) were mixed and allowed to equilibrate with 0.5 mL of the well solution. With the *C. elegans* enzyme, 2.5 μL of the protein solution and 2.5 μL of the correspond-

Table 1
Crystallization conditions used.

System	Concentrations of TS and ligand(s) in the protein solution	Composition of the well solution
*Ts*TS–dUMP	*Ts*TS (20 mg/ml) *dUMP (10 mM)*	0.1 M Tris-HCl pH 7.9 0.08 M $MgCl_2$ 18.5%(w/v) PEG 4000
*Ce*TS	*Ce*TS (23.75 mg/ml) *No ligands*	0.1 M MES pH 5.6 0.15 M $(NH_4)_2SO4$ 18%(w/v) PEG 5000 MME
*Ce*TS–dUMP–Raltitrexed	*Ce*TS (20 mg/ml) dUMP (10.2 mM) Raltitrexed (6.7 mM)	0.1 M Bis-Tris pH 7.0 0.2 M NaAcetate 17%(w/v) PEG 3350

Table 2
Data collection and refinement statistics summary for reported structures.

Crystal and refinement parameters	*T. spiralis* TS–dUMP	*C. elegans* TS	*C. elegans* TS–dUMP–Raltitrexed
PDB ID	**5BY6**[a]	**4IQB**	**5NOO**[b]
Space group	P1	C 2	P 2_1
Unit cell parameters	A = 51.7 Å, b = 65.9 Å, c = 96.5 Å, α = 85.3°, β = 85.3°, γ = 67.1°	a = 99.3 Å, b = 98.4 Å, c = 69.2 Å, β = 111.8°	a = 70.1 Å, b = 94.3 Å, c = 122.1 Å, β = 105.4°
Resolution range [Å]	20–1.90 (1.95–1.90)[c]	30–1.13 (1.16–1.13)	15–2.90 (2.98–2.90)
No. of unique reflections	89350	227936	32822
Completeness [%]	97.3 (88.4)	99.1 (89.5)	96.4 (99.1)
Redundancy	5	3.6	1.8
I/σ(I)	6.1	11.0	4.6
No. of reflections used in refinement	84834	216742	32808
Rfactor [%]	16.5 (24.2)	11.4 (25.5)	21.0 (30.3)
R_{free} factor [%]	22.0 (29.4)	13.9 (28.2)	24.7 (33.6)
RMS bond [Å]	0.018	0.023	0.003
RMS angle [°]	1.82	2.19	0.951
ASU content	Two homodimers	Single homodimer	Two homodimers
Matthews coefficient (solvent content)	2.1 Å^3/Da (42.0%)	1.9 Å^3/Da (34.4%)[d]	2.8 Å^3/Da (56.3%)

[a] Entry **5BY6** supersedes **4G9U** [67].
[b] Entry **5NOO** supersedes **4IQQ**.
[c] Values in parentheses are for highest-resolution shells.
[d] Low solvent content seems to be the cause of the compact arrangement of the protein (the latter reflected by a low temperature factor of 16.7 Å^2 for all atoms in the model).

ing well solution were mixed and allowed to equilibrate with 0.5 mL of the well solution.

X-Ray diffraction data were collected from single flash-frozen crystals either at the BESSY II Synchrotron [68] using an X-ray wavelength of 0.918 Å (*Ts*TS-dUMP and *Ce*TS) or on the SuperNova diffractometer (Oxford Diffraction) using an X-ray wavelength of 1.5418 Å (*Ce*TS-dUMP-Raltitrexed).

2.5. Data processing: structure determination and refinement

Data collected from the *Ts*TS–dUMP and *Ce*TS crystals were processed with DENZO and SCALEPACK [69] and those collected from the *Ce*TS–dUMP–Raltitrexed crystal with CrysAlisPro (Agilent Technologies, Version 1.171.36.20) and SCALA [70]. The structures were determined by molecular replacement carried out with Phaser [71] from the CCP4 package [72], using the following search models: the structure of mouse TS ternary complex with N^4-hydroxy-dCMP and DHF (PDB ID: 4EZ8 [73]) to solve the *Ts*TS–dUMP complex structure, the structure of mouse TS–dUMP–Raltitrexed ternary complex (PDB ID: 4EB4 [54]) to solve the *Ce*TS–dUMP–Raltitrexed complex structure, and the latter *Ce*TS–dUMP–Raltitrexed ternary complex structure to solve the structure of free *Ce*TS. Model refinements and buildings were carried out using Refmac5 [74] and Coot [75], respectively, for *Ts*TS-dUMP and *Ce*TS, and phenix.refine [76] and Coot for *Ce*TS-dUMP-Raltitrexed. The correctness of the final models was evaluated using Sfcheck [77] and Procheck [78] from the CCP4 suite. Selected X-ray data and model refinement parameters are presented in Table 2.

2.6. tCONCOORD computations

In order to generate structural ensembles and evaluate dynamic flexibilities of the systems investigated in this manuscript, tCONCOORD computations [79,80] have been carried out. The method uses a two-step approach to generate the results. First, an original crystal structure is thoroughly minimized, after which it undergoes analysis and subsequent translation into sets of geometrical constraints, consisting of both topological (bonds, angles and ring planarities) and non-covalent ones (hydrogen bonds, hydrophobic clusters and salt bridges). In the process, tCONCOORD employs the default parameter file based on high-resolution X-ray structures from PDB. Next, the structural ensemble is generated employing the topology file of geometrical constrains. To allow a comprehensive inspection of the generated ensembles, RMSF analyses of the ensemble structures have been subsequently performed.

2.7. Amino acid sequences and interface analysis

The following amino acid sequences of TS available at NCBI protein sequences database were used (reported as TS variant – accession code): mTS – NP_067263.1, hTS – NP_001062.1, *Ce*TS – AAC97508.1, *Ts*TS – AAK96220.1. Sequences were compared using rigorous Smith-Waterman search [81,82] with the SSEARCH program available at http://fasta.bioch.virginia.edu/fasta_www2/fasta_list2.shtml. Sequence alignment presented on Fig. 1A was prepared using Clustal Omega [83], and interface residues were identified using PISA [84].

2.8. Molecular docking computations

Several molecular docking computations have been performed in search of ligands differing in predicted binding affinity against thymidylate synthases from nematode (*Ts*TS) compared to mammalian (hTS) species. For this, crystal structures of human (PDB ID: 3N5E [51]) and *T. spiralis* (PDB ID: 5BY6) thymidylate synthases in complexes with a peptide inhibitor LR and dUMP, respectively, were used as receptors. Ligands were removed from both proteins, residues of *S*-methylthio-cysteine present in **3N5E** modeled back to cysteines and missing loops in **3N5E** (residues 120–141 in both chains) generated using Build Loop tool in YASARA v.16.2 [85] and then rebuilt *ab initio* with Rosetta v 3.0 [86,87]. 200 models were generated and sorted using Rosetta total score. 50 best scored models where inspected visually, of which one model was chosen for further experiments. The region of the dimerization interface encompassing several non-conserved residues such as *Ts*TS Tyr152, Thr174, Cys191 and Phe192 (or equivalent hTS Val158, Cys180, Ala197 and Leu198, respectively) and forming a large cavity was chosen as the docking site (Fig. 1). The Cα-RMSD between the whole dimerization interfaces of the human and *T. spiralis* structures or between their parts, consisting of residues forming the docking sites, amount to 1.8 Å or 0.7 Å (both values calculated with MUSTANG [88]), respectively, indicating on the one hand an effect of

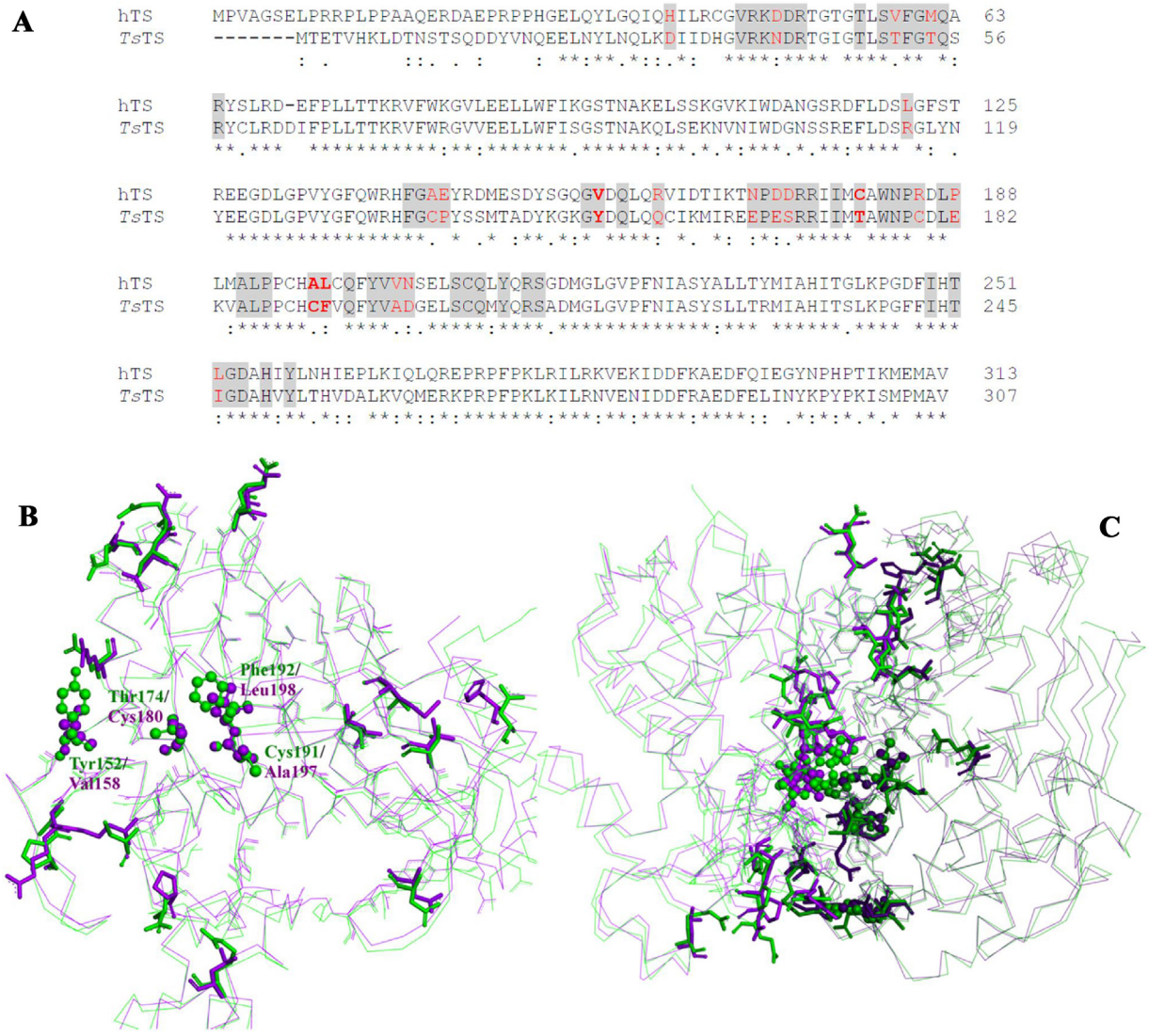

Fig. 1. Dimerization interface. [A] Alignment of human and *T. spiralis* TS sequences in single subunit. Interface residues are highlighted in gray. Non-conserved interface residues are depicted in red and those involved in interactions with ligands additionally highlighted in bold. Note that due to TS being a symmetric homodimer, the dimerization interface is composed from the same sets of residues from both subunits. [B] Side-view of hTS (violet) and *Ts*TS (green) monomers. Non-conserved residues in the dimerization interface are shown in stick and those involved in interactions with ligands in ball and stick. [C] Their localization in both subunits of complete TS dimer.

enhanced similarity at the docking site, but on the other hand a more differentiated structural surroundings of it. Fig. S1 in Supplementary Material shows the complete dimers of **3N5E** and **5BY6** colored according to RMSF, calculated based on structural ensembles from the simulations carried out with tCONCOORD. Although some differences are visible, the dimerization interfaces are colored almost identically in both structures, indicating no differences in flexibility. Together, the differences between the dimerization interfaces and, especially, docking sites in the structures of human and *T. spiralis* TS receptors were not of a caliber to disallow reliable comparative docking computations, where the differences in AA composition would play no lesser role than different conformations of the starting models.

Receptor preparation including assigning of atomic charges, optimizing the orientation of hydroxyl groups in Asn and Gln residues, protonation states in His residues, and minimization, was handled with Protein Preparation Wizard from the Small-Molecule Drug Discovery Suite (S-MDDS) 2015-3 (Schrodinger, LLC, New York, NY, 2015). Ligands were downloaded from the non-commercial small-molecule libraries (subsets of ZINC15 [89], Specs [https://www.specs.net/], and Asinex [http://www.asinex.com/] databases were used, as well as entire NuBBE [90], and TCM Database@Taiwan [91] databases). The libraries were filtered with MONA [92,93] to eliminate duplicates. Ligand preparation for docking was performed with LigPrep from S-MDDS and consisted of a series of steps, including applying corrections to the structure and generating ionization states and tautomers. Preparations were completed with the receptor-ligand complex refinement carried out by minimizing the side chains and keeping the backbone atoms restrained. Docking experiments were performed using BioSolveIT software packages (BioSolveIT GmbH, Sankt Augustin, Germany). 20 best poses from FlexX docking [94] invoked via LeadIT 2.2.0 were re-scored using HYDE scoring function [95,96] implemented in SeeSAR 5.4. Ligands with the best HYDE affinity and favorable torsion angles were allocated to the next step of the filtering procedure, consisting of the MD and MM-GBSA computations.

2.9. Molecular dynamics (MD) simulations

The most promising poses from docking, deemed as such based on high docking scores and more favorable binding to *Ts*TS than hTS, have been subjected to molecular dynamics runs to assess

the stability of receptor-ligand complexes. The poses were first neutralized with sodium counter-ions and explicitly solvated in a truncated octaedric box of TIP3P water molecules [97] extended up to 8 Å from the outer protein wall. All simulations were performed with the GPU version of the pmemd module of AMBER 14 molecular dynamics package [98] using the ff14SB force field parameters [99] for the proteins atoms and GAFF parameters [100] coupled with semi-empirical AM1-BCC charges [101,102] for the ligands atoms. Energy minimizations were carried out in two steps, first with solute atoms held fixed, followed by the minimization of the whole system, using the steepest-descent and conjugate-gradient algorithms. Gradual heatings were carried out in two intervals, firstly 0–50 K (10 ps) and afterwards 50–300 K (20 ps). Temperature was increased linearly as a function of time in both periods and the weak positional restraints were applied to the backbone atoms. This was followed by the equilibrations lasting for 100 ps and data collection runs for 10 ns. The NpT ensemble (conserved number of atoms N, pressure p and temperature T) and periodic boundary conditions were applied throughout the simulations. The temperature and pressure were maintained at 300 K and 1 atm using the Langevin thermostat [103] and the isotropic position scaling with Monte Carlo barostat, respectively, with both coupling times of 1 ps. A 2 fs integration time step and the SHAKE algorithm [104] with a relative tolerance of 0.00001 Å to constrain bonds connecting to hydrogen atoms were applied. Long-range Lennard-Jones and electrostatic interactions were evaluated using the particle-mesh Ewald (PME) method [105,106]. A charge grid spacing of approximately 0.9 Å was used. The charge grid was interpolated using a cubic β-spline of the order of 4 with the direct sum tolerance of 0.00001 at the 8 Å direct space cutoff. During data collection runs the coordinates were saved every 2nd ps for further analyzing, yielding 5000 frames from each run. RMSD and RMSF of the main chain atoms were evaluated with the cpptraj module of AMBER 14. The occurrence of hydrogen bonding was assessed using the donor-acceptor distance and donor-hydrogen-acceptor angle cutoffs of 3.2 Å and 120°, respectively.

2.10. Free energy of binding computations

In order to re-rank the binding affinities predicted in the docking experiments, the trajectories from MD simulations of the docking poses have been subjected to the receptor-ligand binding free energy computations carried out using the Molecular Mechanics-Generalized Born Surface Area (MM-GBSA) approach [107]. In MM-GBSA, the binding free energy is defined as the free energy difference between the bound state (complex) and the unbound state (receptor + ligand) in aqueous solution: $\Delta G_{bind} = \Delta G(complex)_{aq} - \Delta G(receptor)_{aq} - \Delta G(ligand)_{aq}$. Since ΔG_{bind} is calculated with the thermodynamic cycle, it can be expressed as: $\Delta G_{bind} = \Delta E_{mm} + \Delta G_{solv} - T\Delta S_{solute}$, where ΔE_{mm}, ΔG_{solv} and $T\Delta S_{solute}$ are the ΔG_{bind} contributions from the molecular mechanics energy, solvation free energy and solute entropy, respectively. ΔE_{mm} can be expressed as the sum of changes in the electrostatic, van der Waals and internal energies in the gas-phase ($\Delta E_{mm} = \Delta E_{ele} + \Delta E_{vdW} + \Delta E_{int}$, respectively), whereas ΔG_{solv} as the sum of changes in the polar and non-polar solvation free energies ($\Delta G_{solv} = \Delta G_{GB} + \Delta G_{np}$, respectively). The solute entropies were not calculated in this work due to known difficulties in their accurate assessment and debated contribution to the free energy [108]. The work-flow of the computations was as follows: after discarding water and counter-ions, molecular mechanics energies for the complex, receptor and ligand were calculated using a dielectric constant of 1 and an infinite cutoff for all interactions. Polar solvation free energies for the complex, receptor and ligand were calculated using a continuum representation of the solvent and the modified generalized Born (GB) solvation model II [109]. Dielectric constants of 1 and 78.5 were assigned to the solute and solvent, respectively. Non-polar solvation free energies for the complex, receptor and ligand were evaluated from the solvent accessible surface area (SASA) with the LCPO method [110]. Decomposition of the binding free energies on a per-residue basis was conducted in order to prioritize between different receptor-ligand interactions. All calculations were performed using the tools from AMBER 14 package: the *MMGBSA.py* script and the SANDER program.

2.11. Accession numbers

Atomic coordinates and structure factors for the reported crystal structures have been deposited in the Protein Data Bank under accession codes 5BY6 (*Ts*TS-dUMP), 4IQB (*Ce*TS) and **5NOO** (*Ce*TS-dUMP-Raltitrexed).

3. Results and discussion

3.1. High-resolution structure of the unliganded CeTS protein

After an initial refinement, numerous peaks on the difference electron density map indicated locations in which hydrogen atoms of the protein would be expected. These hydrogen atoms, included in the course of refinement, are not shown in the final model due to their irregular occurrence on the map. At the later stages of the model refinement, the anisotropic temperature factors were applied. The final model encompasses a large 288-residual segment of the enzyme (Gln24–Met311). Similar to the remaining structures presented here, the 50–54 loop is partially disordered and exhibits a high temperature factor of 73 $Å^2$, compared to an average value of 16.7 $Å^2$ for the whole polypeptide chain. The terminal segments, Met1–Gln23 (N-terminus) and Asp312–Val315 (C-terminus), were too much disordered to be considered reliable and included in the final model. Of note is that the N-terminus is usually disordered, and therefore absent in the crystal structures of metazoan thymidylate synthases. The only exception was the structure of mouse TS in a complex with dUMP and Raltitrexed (PDB ID: 4EB4 [54]), wherein the 1–13 N-terminal segment was found ordered to the point of generating an unambiguous electron density. The segment was apparently stabilized by contacts with other molecules of the enzyme in the asymmetric unit.

3.2. Structure of the TsTS–dUMP binary complex

The structure of *Trichinella spiralis* thymidylate synthase-dUMP complex encompasses two dimers, AB and CD, comprising of amino acid residues 17–300 and 17–304 (subunits A and B, respectively), and 18–303 and 18–299 (subunits C and D, respectively). All residues in the final model are found within the most favored (91.4%) or additional allowed (8.6%) regions of the Ramachandran plot (not shown). The electron density is less clear in the region 41–46 in all subunits and in the region 109–122 in subunits B and C. It is overall well defined for the substrate molecule in all subunits. The distances between C6 of the pyrimidine ring and γS of the catalytic Cys197 are on average ~3.5 Å, indicating the lack of covalent bond. The AB and CD dimers in the *Ts*TS–dUMP complex show a high degree of similarity to each other, reflected by the root-mean-square-deviation (RMSD) value of 0.29 Å for the backbone Cα atoms. The subunits A and B, as well as C and D, are also closely similar to each other, reflected in the Cα RMSD of 0.39 and 0.28 Å, respectively. Nevertheless, the subunit B adopts a slightly more closed conformation compared to the subunit A due to the loop Lys40–Thr48 and the C-terminus covering the active site cleft to a slightly larger extent in the former than in the latter subunit.

3.3. Structure of the CeTS-dUMP-Raltitrexed ternary complex

The structure of the *Ce*TS–dUMP–Raltitrexed complex encompasses two dimers, AB and CD, comprising of amino acid residues 24–310 (subunits A, B and C) and 26–312 (subunit D). A comparison of the four subunits present in the asymmetric unit indicates only slight conformational differences concerning the mobile C- and N-termini and the surface loop Asp50–Thr54 (the Asp50-Thr52 and Arg51 residues are absent in subunits C and D, respectively, due to very poor electron densities). The partially disordered C-terminus and the loosely bound molecule of Raltitrexed point to the active site of the enzyme being only partially closed. The electron density is clear for the ligands, dUMP and Raltitrexed, having their pyrimidine (dUMP) and quinazoline (Raltitrexed) rings aligned parallel to each other.

The catalytic Cys197 and the dUMP pyrimidine ring C6 are located in each subunit at a distance (3.5 Å on average in four subunits) precluding the covalent linkage. Overall, the dUMP molecule is coordinated by the enzyme in a typical way, i.e. by hydrogen bonds between dUMP uracil O2 and Asp220, dUMP uracil O4

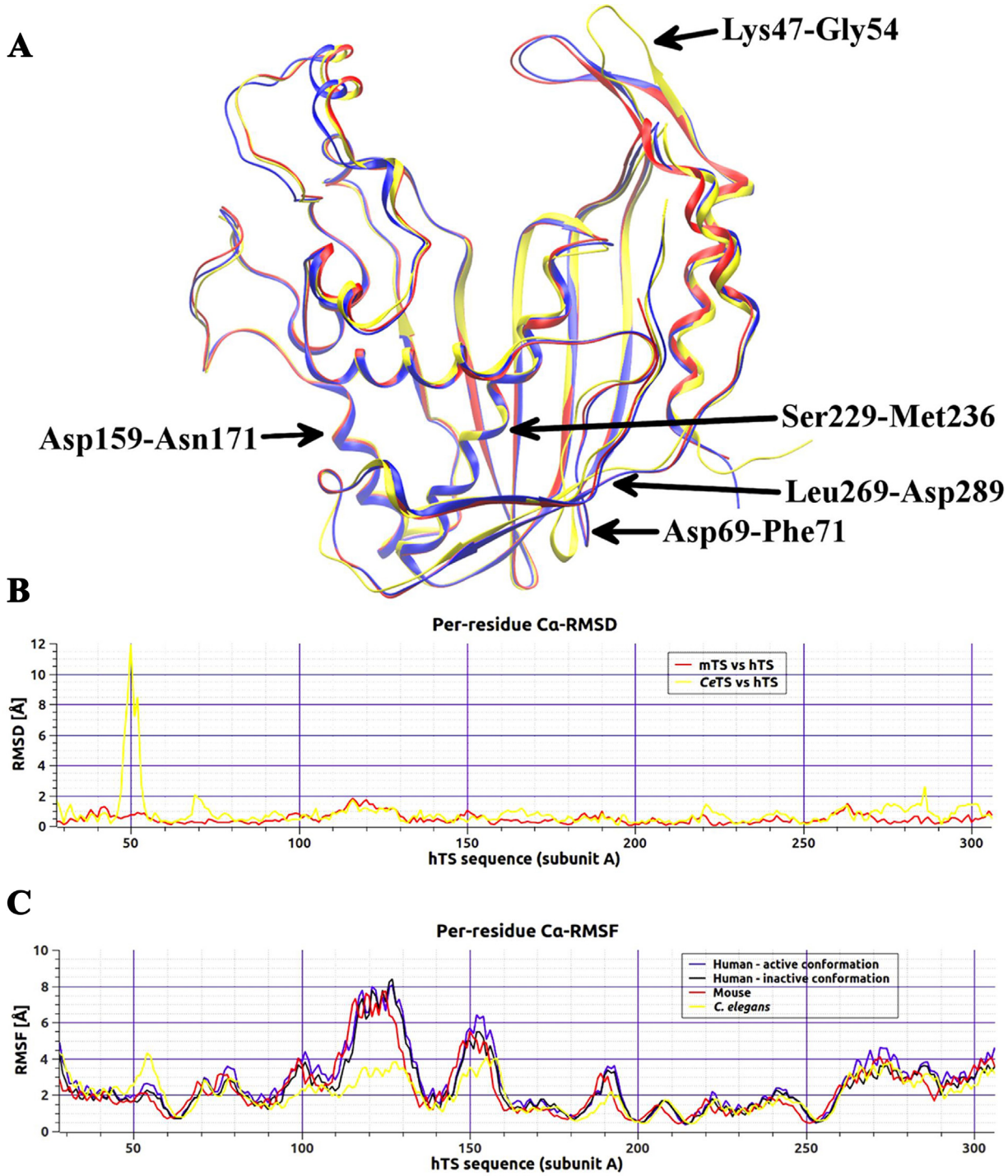

Fig. 2. [A] Structural alignment of subunits A from the ligand-free structures of hTS (blue), mTS (red) and *Ce*TS (yellow). Nomenclature according to the sequence of the human enzyme. [B] Per-residue Cα RMSD in subunits A. [C] Per-residue Cα RMSF in subunits A. (For interpretation of the references to colour in this figure legend, the reader is referred to the web version of this article.)

and N3-H and Asn228, dUMP deoxyribose O3′-H and His258 and Tyr260, dUMP phosphate group and the quartet of arginines (51, 217, 177′, 178′) and single serine (218). The Raltitrexed molecule is linked by hydrogen bonds from N3 to the side chain of Asp220 and from O4 to the main chain of Gly224. Of note is, though, that the glutamate part of Raltitrexed is poorly coordinated by the enzyme.

3.4. *Comparison of the ligand-free structures of* C. elegans, *mouse and human thymidylate synthases*

The amino acid sequences of hTS and mTS show a high degree of homology, while the sequence of *Ce*TS differs from them more significantly (Table 3). The Cα RMSD for the whole dimeric structures are 0.7, 1.3 and 1.3 Å between hTS (PDB ID: 4UP1) and mTS (PDB ID: 3IHI), hTS and *Ce*TS (PDB ID: 4IQB) and mTS and *Ce*TS, respectively, indicating a very strong structural "consensus" between the two ligand-free mammalian enzymes and almost two-times worse between each of them and the ligand-free nematode enzyme. The most evident differences in the per-residue RMSD plot, depicted also on the 3D structural superposition of the ligand-free hTS, mTS and *Ce*TS structures (Fig. 2B and A, respectively) pertain to (i) the loop Arg48–Gly55 (according to the *Ce*TS sequence), which is in a largely different conformation in *Ce*TS compared to both mammalian enzymes, (ii) a region in a loop adjacent to the second strand (Gly54-Ser66 in the hTS sequence or Gly55-Cys67 in the *Ce*TS sequence) of the central β-sheet, where a single aspartate in the hTS sequence, Asp69, has an equivalent in an asparagine-glycine couple in the *Ce*TS sequence (Asn70-Gly71), (iii) the surface AA8 helix Asp161-Gln173 (according to the *Ce*TS sequence; for the secondary structure nomenclature, see Fig. 3 and its legend), (iv) the Ser231-

Table 3
Comparison of TS amino acid sequences. Values show percent of identity and percent of similarity (in brackets).

	hTS	mTS	*Ce*TS	*Ts*TS[a]
hTS	–	88.8 (94.9)	68.1 (86.7)	68.8 (88.8)
mTS	88.8 (94.9)	–	67.4 (86.3)	67.4 (87.7)
*Ce*TS	68.1 (86.7)	67.4 (86.3)	–	60.5 (85.5)
*Ts*TS	68.8 (88.8)	67.4 (87.7)	60.5 (85.5)	–

[a] Comparison of the *Ts*TS-dUMP complex with other binary complexes of TS is presented in another section of Results and discussion, but the comparison of *Ts*TS sequence is included in this Table for the convenience of the reader.

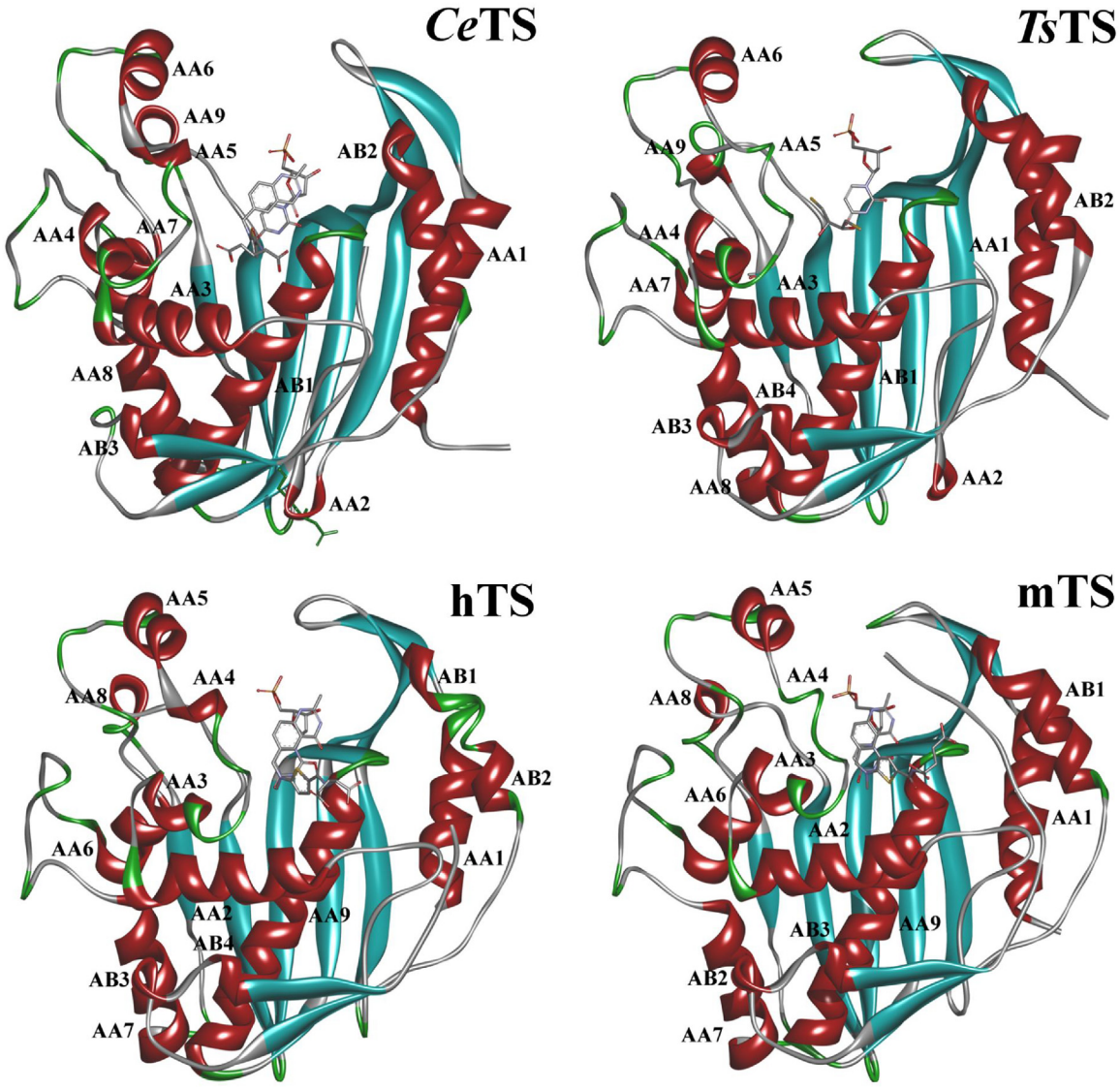

Fig. 3. Nomenclature of the secondary structure elements in subunit A of the *Ce*TS (5NOO), *Ts*TS (5BY6), hTS (1I00) and mTS (4EB4) structures. All α-helices are labeled. β-sheets are colored blue. In the structural arrangement shown, the strands in the central 6-stranded β-sheet are numbered from right to left (numbers not shown).

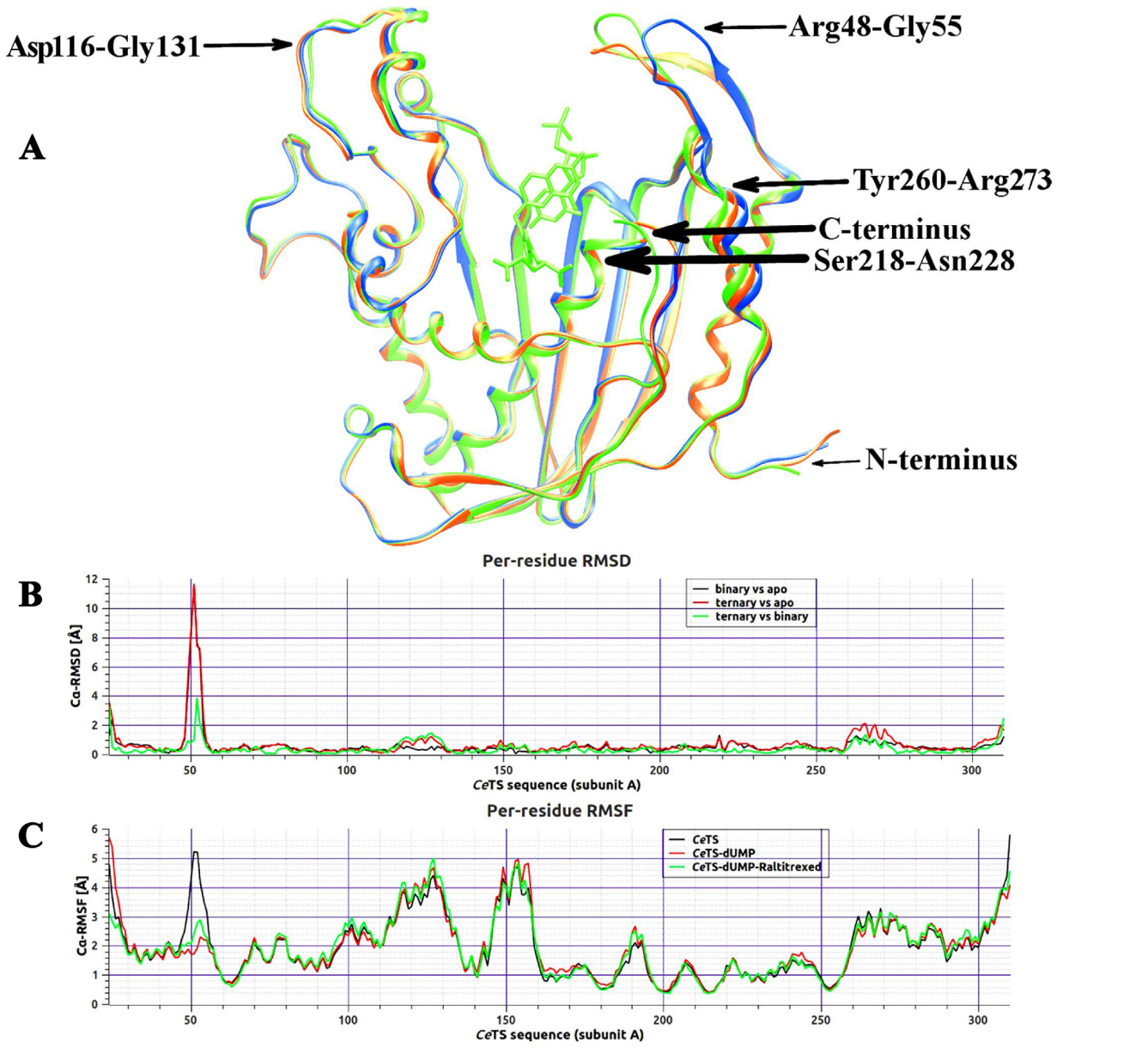

Fig. 4. [A] Structural alignment of subunits A from the ligand-free *Ce*TS (blue), the *Ce*TS-dUMP complex (orange) and the *Ce*TS-dUMP-Raltitrexed complex (green). [B] **Per-residue Cα RMSD in subunits A. [C] Per-residue Cα RMSF in subunits A**. (For interpretation of the references to colour in this figure legend, the reader is referred to the web version of this article.)

Met238 middle segment of the central AB1 helix, and (v) the long circular loop Leu271-Asp291.

In the absence of the substrate and cofactor, the Ala181–Leu198 loop in human TS (Ala183–Leu200 in *Ce*TS) can adopt two alternative conformations, differing by a 180° rotation, with the catalytic cysteine located either in the active site, adjacently to the binding site of dUMP (active conformation), or pushed outside the active site (inactive conformation). It has been shown that the inactive conformation of human TS is stabilized due to the presence of double hydrogen bonding between the side chain of Arg163 and the carbonyl oxygens of Ala191 and Leu192 [43]. Replacement of arginine with lysine in mouse TS (Lys157 in place of Arg163) prevents formation of the inactive conformer due to structural conditions forestalling the hydrogen bonding with lysine [111]. Replacement of arginine with glutamate in *Ce*TS (Glu165 in place of Arg163) preserves the effect of replacement with lysine and causes the nematode enzyme to populate the active conformation.

3.5. Comparison of the unliganded CeTS with its binary and ternary complexes

Differences were sought between the structures of ligand-free *Ce*TS and its complexes with dUMP and both dUMP and Raltitrexed, using a multiple structural alignment generated by MUSTANG for a portion of the polypeptide chain present in all three models (residues 25–311). The resulting superposition is shown in Fig. 4A. The Cα RMSD for the dimeric structures are 1.0, 1.0 and 0.5 Å between *Ce*TS and *Ce*TS-dUMP, *Ce*TS and *Ce*TS–dUMP–Raltitrexed and *Ce*TS–dUMP and *Ce*TS–dUMP–Raltitrexed, respectively, indicating less pronounced differences between the two liganded forms of *Ce*TS than between either one of them and ligand-free *Ce*TS. The per-residue RMSD plot, depicting local structural differences in 2D space, is shown in Fig. 4B. The largest RMSDs are apparent for fragments characterized by poor electron densities: the C- and N-termini and the loop Arg48–Gly55, localized on one flank

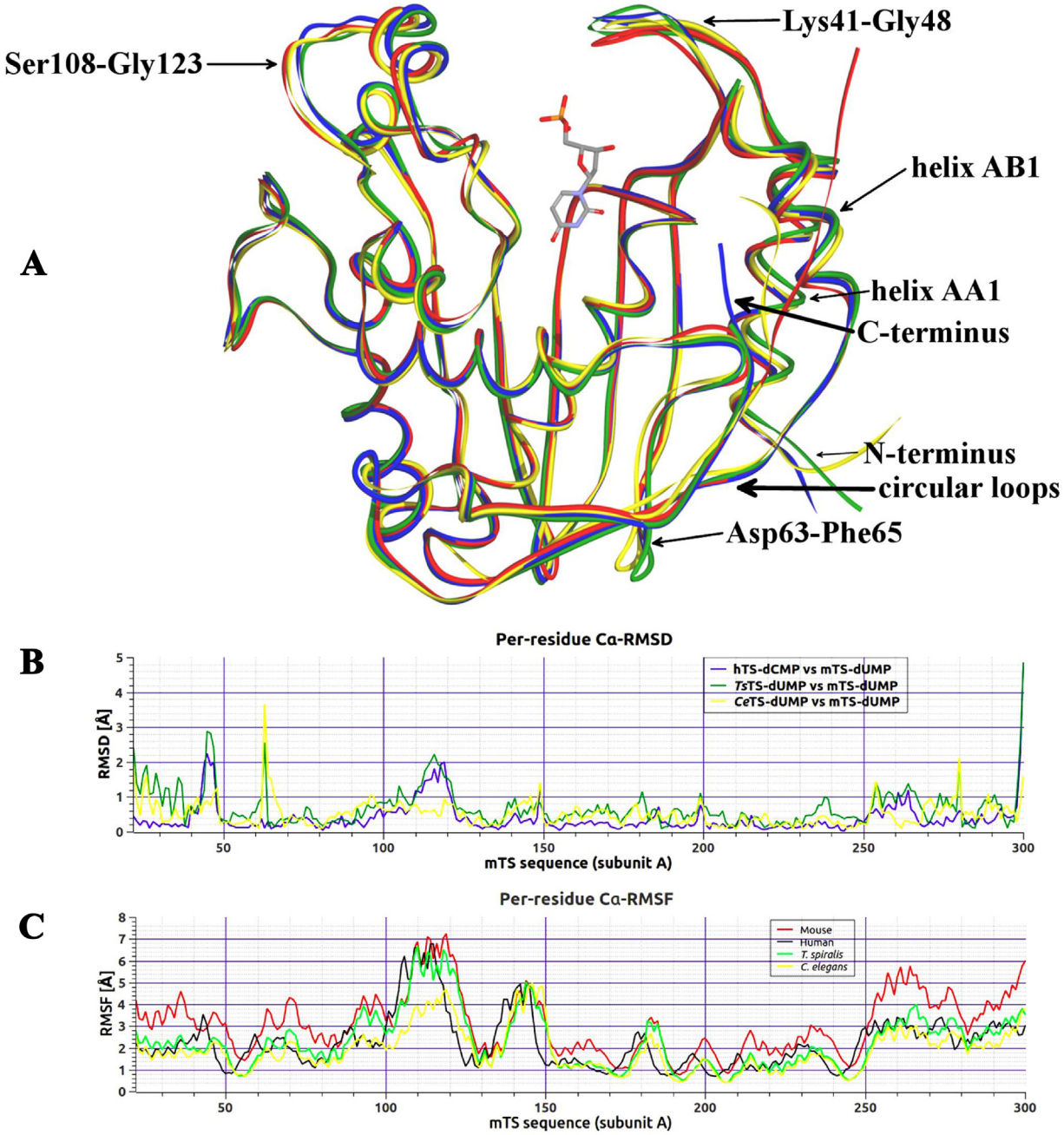

Fig. 5. [A] Structural alignment of subunits A from the dUMP-bound complexes of mTS (red), *Ts*TS (green) and *Ce*TS (yellow) and subunit B from the dCMP-bound complex of hTS (blue). Nomenclature according to the sequence of the mouse enzyme. [B] **Per-residue Cα RMSD in subunits A. [C] Per-residue Cα RMSF in subunits A.** (For interpretation of the references to colour in this figure legend, the reader is referred to the web version of this article.)

of the entrance to the active site pocket and containing Arg51, a residue participating in hydrogen bonding of the phosphate moiety of dUMP. In the ligand-free enzyme, this loop is pointing away from the active site, and thus contributes to its open state. Upon binding of dUMP, and later Raltitrexed, the loop flips inwards the active site, forming in the binary and ternary (dimer AB) complexes a hydrogen bond with the phosphate moiety of dUMP. Smaller but still distinct shifts from the positions occupied in the ligand-free enzyme, reflected in the RMSD values in the range of 1.5–2.0 Å (Fig. 4B), pertain to three other segments of the polypeptide chain in the ligand-bound complexes, all placed in the proximity of the active site. One such difference can be seen in the loop Ser218–Gly222 and the adjacent α-helical segment Leu223–Asn228, which together encompass two residues participating in hydrogen bonding of dUMP: Ser218 (hydrogen bond with the phosphate moiety) and Asn228 (two hydrogen bonds with N3–H and O4 of the uracil moiety). Another distinct RMSD shift concerns the segment Ser261–Leu271 (containing α-helix AB2), adjacent and contributing to an outer shell surrounding the active site. As a consequence of Tyr260 and His258 involvement in hydrogen bonding of the 3′-OH group of the deoxyribose moiety of dUMP, this segment progressively shifts toward the active site. The effect is initiated upon binding of dUMP in the binary complex [67] and reinforced upon binding of Raltitrexed in the ternary complex. Finally, a strictly specific effect of the binding of Raltitrexed is apparent for the AA6 helix-loop segment Asp116–Gly131, localized on the

opposite flank of the entrance to the active site pocket (in relation to the loop Arg48–Gly55) and shifted toward the active site in the *Ce*TS–dUMP–Raltitrexed complex, but not upon the binding of dUMP in the *Ce*TS–dUMP complex, where this segment moves very slightly and nearly retains its position from the ligand-free structure. However, the movement of the segment 116–131 does not seem to participate in the binding of Raltitrexed, but rather, together with the displacement of the loop 48–55, in partially sealing the active site in the ternary complex, thus contributing to its semi-closure. The closure of the active site is normally accompanied by a movement of the C-terminus [25], although this effect cannot be fully exploited here because of the C-terminus being disordered and therefore partially absent in the final models of the ligand-free and ligand-bound structures. Quite expectedly though, the sum of conformational changes, caused by the binding of dUMP alone, is lesser and not conducive toward a semi-closed state, as in the case of the binding of both dUMP and Raltitrexed in the ternary complex.

The distances between C6 of dUMP and γS of Cys197 rule out the possibility of a covalent linkage between the substrate and enzyme in both the *Ce*TS–dUMP–Raltitrexed (3.5 Å on average) and the *Ce*TS–dUMP (3.3 Å) [67] structures. In accord, the dUMP molecule occupies the same position in both ligand-bound structures. The position is secured by several hydrogen bonds to the phosphate, deoxyribose and uracil moieties as well as, exclusively in the ternary complex, by hydrophobic stacking between the dUMP pyrimidine and Raltitrexed quinazoline rings.

The active site of each *Ce*TS subunit contains a single sulfate anion, located similarly as the phosphate group of dUMP in the *Ce*TS–dUMP and *Ce*TS–dUMP–Raltitrexed complexes. The same was previously observed for the corresponding mouse (PDB ID: 3IHI [111]) and human (PDB ID: 4H1I [112]) enzyme structures. The sulfate anions in the *Ce*TS structure are loosely bound by the protein, as indicated by their relatively high temperature factors (45 and 37 Å^2 in subunits A and B, respectively), distinctly exceeding the average isotropic temperature factor for the whole model (16.7 Å^2). Their positions are stabilized by hydrogen bonds with two arginine residues, Arg217 and Arg178′, both participating in hydrogen bonding of the phosphate moiety of dUMP in both liganded forms of *Ce*TS. It should be noted that in the absence of dUMP, some amino acid residues engaged in its binding in liganded forms of the enzyme, including Ser218, catalytic Cys197 and Arg178′, are less ordered and adopt two alternative conformations.

3.6. *Comparison of* T. spiralis, C. elegans, *mouse and human thymidylate synthases in binary complexes with either dUMP or dCMP*

In search of unique fragments distinguishing the nematode from mammalian TSs, a thorough comparison between the structures of *Ts*TS–dUMP and *Ce*TS–dUMP and the analogous structures of mTS–dUMP (PDB ID: 4E5O [111]) and hTS-dCMP (PDB ID: 5WRN; not published yet) was conducted. Note that the hTS-dCMP structure was accepted for comparison in view of the lack in PDB of the hTS-dUMP structure.

The amino acid sequences of mTS, hTS, *Ts*TS and *Ce*TS show a decent degree of homology, with the one between hTS and mTS being significantly larger compared with the remaining sequences (Table 3). On the other hand, differences between *Ce*TS and *Ts*TS are the largest among all compared sequences. This can be attributed to, often overlooked, diversity of nematodes [113], especially considering relatively large evolutionary distance between *C. elegans* belonging to the clade V of Nematoda and *T. spiralis* from clade I [114–116]. Since most of the sequence differences pertain to amino acids of the same character, the local hydrogen bonding and/or hydrophobic interactions are mostly preserved, regardless of the enzyme origin. Moreover, the comparison of 3D-structures of *Ts*TS-dUMP, *Ce*TS-dUMP, mTS-dUMP and hTS-dCMP by means of superposition (Fig. 5A) showed an overall high structural similarity, with the Cα RMSD for the whole dimeric structures amounting to between 0.6-0.8 Å between each of the four structures, and the per-residue RMSD rarely reaching or exceeding 1.5–2 Å (Fig. 5B). The most substantial difference in the RMSD plot pertains to a peripheral region in a loop nearby the second strand of the central β-sheet, where a single aspartate in the mTS sequence (Asp63), or hTS sequence (Asp69), has an equivalent in two aspartate residues in the *Ts*TS sequence, Asp62 and Asp63, or in an asparagine-glycine couple in the *Ce*TS sequence, Asn70-Gly71. Together, the neighboring sequences in this region are different in both length and composition in the mammalian (Asp63-Glu64-Phe65 in the mTS sequence and Asp69-Glu70-Phe71 in the hTS sequence) compared to nematode enzymes (Asp62-Asp63-Ile64-Phe65 in the *Ts*TS sequence and Asn70-Gly71-Thr72-Ile73 in the *Ce*TS sequence), resulting in a local conformational diversification, reflected in the high RMSD peaks observed for this region in the *Ce*TS-dUMP vs mTS-dUMP and *Ts*TS-dUMP vs mTS-dUMP profiles. However, as the region is distant from both the active site and the dimerization interface, it seems not likely to contribute to the inhibitory arsenal searched for in this paper. Other relatively large differences in the RMSD plots pertain to (i) a large segment from the N-terminus through the AA1 helix (Asn20-Gly37) and the first strand (Val38-Asn41) of the central β-sheet to the loop Asp42-Ile46 (according to the *Ts*TS sequence), flanking one of the entrances to the active site, and, treated as a whole, but with lower absolute RMSD numbers and several residues within showing small RMSD differences, (ii) another large segment, consisting (in the reverse order of sequence numbering) of the C-terminus, extended circular loops, the AB4, AB3 and AB2 helices and a few residues in an outer shell surrounding the active site, including Tyr252. One of the sharpest peaks in the RMSD plot concerns *Ts*TS Arg115 from the AA6 helix-loop segment 108–123 flanking the other entrance to the active site. Replacement of Arg115 in *Ts*TS-dUMP with Leu115 in mTS-dUMP, Leu121 in hTS-dCMP or Leu123 in *Ce*TS-dUMP results in a loss of two hydrogen bonds, linking in the *Ts*TS-dUMP structure Arg115 with Val184 from a different part of the polypeptide chain. On the other hand, a strong AA conservation and modest RMSD shifts can be observed within the active site, although some conformational differences are still apparent there. The most interesting difference concerns the position of *Ts*TS His190 (His190 in mTS, His196 in hTS and His198 in *Ce*TS). In the mTS–dUMP structure the side chain of His190 is located at a hydrogen bonding distance from the dUMP O4 atom. In the hTS-dCMP structure the side chain of His196 is located similarly as in the mTS-dUMP structure, however, being not engaged in hydrogen bonding with dCMP. In the *Ce*TS–dUMP structure the side chain of His198 is flipped over and slightly shifted, such that it prevents H-bond formation with dUMP. A conformation similar to the latter one can also be observed for homologous His147 in the *E. coli* TS complex with dUMP (*Ec*TS-dUMP; PDB ID: 1BID [117]). At last, His190 in the *Ts*TS–dUMP structure adopts two alternative, yet similarly occupied conformations, one similar to the conformation present in the mTS–dUMP and hTS-dCMP structures and the other to the conformations encountered in the *Ce*TS–dUMP and *Ec*TS–dUMP structures. Another difference concerns the position of *Ce*TS Asn228 (Asn220 in *Ts*TS and mTS or Asn226 in hTS). Here, a small bending of the dUMP pyrimidine ring, observed in the *Ce*TS–dUMP structure, but not in the *Ts*TS–dUMP, mTS–dUMP and hTS-dCMP structures, results in the N—H group of the side chain of Asn228 being shifted by about 1.2 Å in order to preserve hydrogen bonding with the uracil O(4) atom.

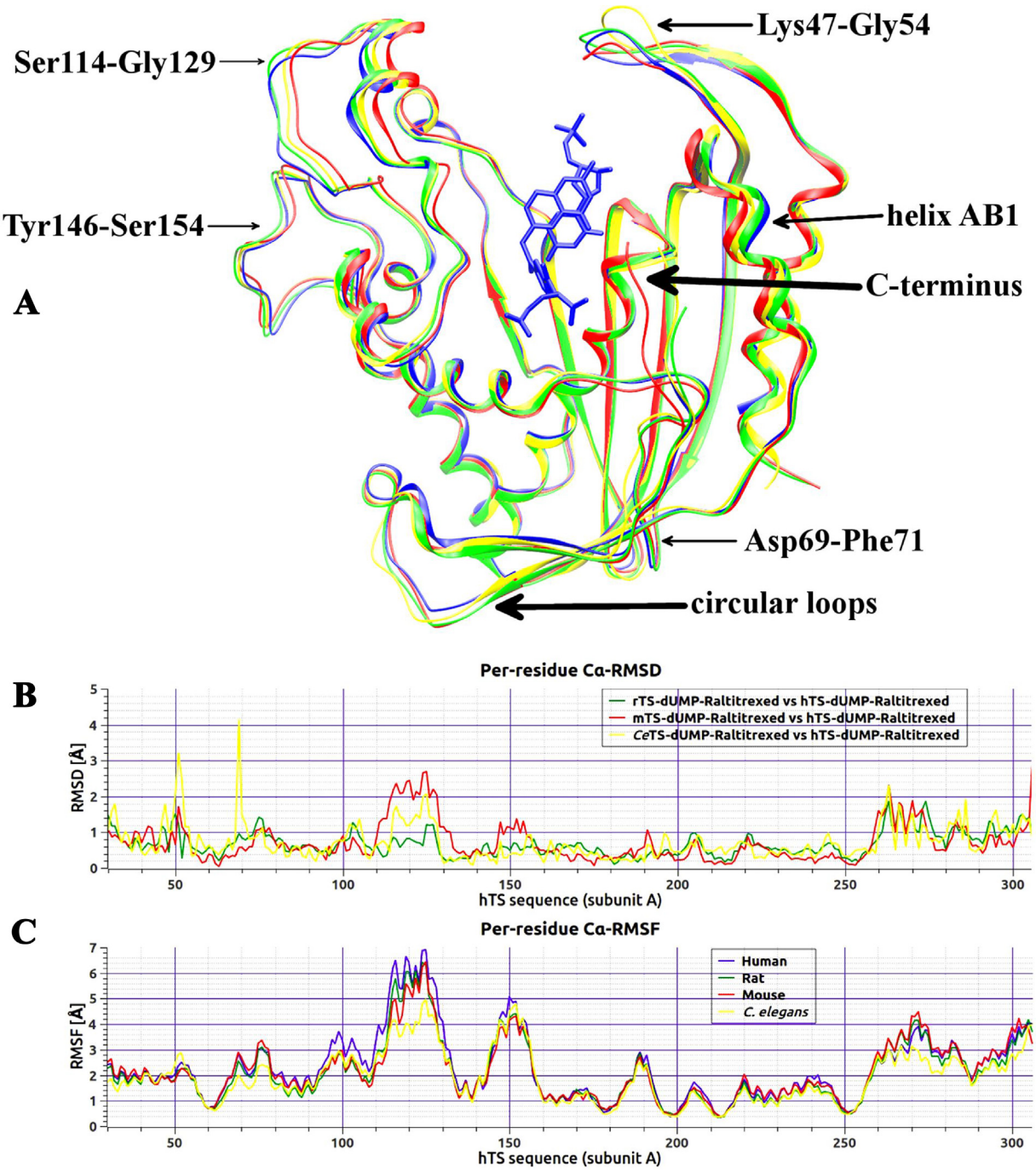

Fig. 6. [A] Structural alignment of subunits A from the dUMP- and Raltitrexed-bound complexes of hTS (blue), rTS (green), mTS (red) and *Ce*TS (yellow). Nomenclature according to the sequence of the human enzyme. [B] **Per-residue Cα RMSD in subunits A. [C] Per-residue Cα RMSF in subunits A.** (For interpretation of the references to colour in this figure legend, the reader is referred to the web version of this article.)

3.7. *Comparison of* C. elegans*, mouse, rat and human thymidylate synthases in ternary complexes with dUMP and Raltitrexed*

Almost all structures of TS ternary complexes present in the Protein Data Bank show the enzyme in either closed (hTS, PDB ID: 1HVY [42]; *Ec*TS, PDB ID: 2KCE [118]) or open (hTS, PDB ID: 1I00 [44]; rat TS, PDB ID: 2TSR [53]) conformations, with the former conformation accompanied by dUMP and the catalytic cysteine covalently bonded and the C-terminus covering the active site, and the latter showing dUMP and the catalytic cysteine separated and the C-terminus disordered. Unlike these two "generic" conformations, the structure of the ternary complex of mouse TS (PDB ID: 4EB4 [54]) shows the enzyme in the mixed conformation (more closed in one dimer (AB) and more open in the other (CD)), with dUMP and the catalytic cysteine relatively close to each other, but not enough to form the covalent bond. The present ternary complex of *Ce*TS (PDB ID: 5NOO) reveals yet another, though similar, conformation, with the active site semi-closed, and dUMP and the catalytic cysteine separated.

Amidst the two generic conformations of the ternary complexes of human TS with dUMP and Raltitrexed, represented by the structures **1HVY** and **1I00**, the latter conformation is more similar to the semi-closed state of the enzyme, present in the conformations of

the *Ce*TS–dUMP–Raltitrexed (**5NOO**) and mTS–dUMP–Raltitrexed (**4EB4**) structures. Eventually, since in the rTS-dUMP-Raltitrexed structure **2TSR** the enzyme populates the same conformational state compared to the structure **1I00**, a comparison was made between the **5NOO**, **4EB4**, **1I00** and **2TSR** structures.

The amino acid sequences of mammalian (human, rat and mouse) and nematode (*C. elegans*) TS show a high degree of homology, reflected in the sequence identity and similarity scores of 59.5 and 85.6%, respectively, between all four sequences. The comparison of 3D-structures of the ternary complexes (with dUMP and Raltitrexed) of *Ce*TS, hTS, mTS and rTS by means of superposition (Fig. 6A) showed a comparable structural similarity compared to the one observed for the binary complexes, with the Cα RMSD for the whole dimeric structures amounting to between 0.6 and 1.0 Å for each pair of structures and the per-residue RMSD for the corresponding amino acid residues rarely reaching or exceeding 1.5–2 Å (Fig. 6B). Like with the RMSD plot for the structures of binary complexes (Fig. 5B), the most substantial differences in the plot in Fig. 6B pertain to (i) a region in a loop adjacent to the second strand of the central β-sheet, where a single aspartate in the sequence of mammalian enzymes (Asp69 in hTS or Asp63 in mTS and rTS), has a replacement in an asparagine-glycine pair in the *Ce*TS sequence, Asn70-Gly71, which implicates local conformational changes in the nematode enzyme in comparison with the mammalian enzymes, (ii) a large segment 255–306 (according to the hTS sequence) consisting (in the reverse order of sequence numbering) of the C-terminus, extended circular loops, the AB4, AB3, AB2 and AB1 helices and a few residues belonging to the third strand (255–258) of the central β-sheet and embedded in an outer shell surrounding the active site, and (iii) the active site flanking loop Arg48-Gly55 (according to the *Ce*TS sequence). In the *Ce*TS-dUMP-Raltitrexed complex the loop 48–55 seals the active site lesser than the homologous loops in the mammalian ternary complexes, resulting in a less closed state of the enzyme active site in the former compared to the latter complexes. Another distinct RMSD difference, which adds up with the difference discussed just above, concerns the other active site flanking segment, AA5 helix-loop Ser114-Gly129 (according to the hTS sequence), which extends unevenly inwards the active site in the four analyzed complexes, with the largest shift (most closed AS entrance) in each subunit pertaining to the mouse enzyme and the smallest shift (least closed AS entrance) to subunit B of the nematode enzyme. Finally, a smaller yet still evident RMSD difference pertains to the surface loop Tyr140-Ser148 (according to the mTS sequence) located in the proximity of the AA6 and AA7 helices, the position of which in subunit A of the mTS complex differs on average by about 0.5–0.8 Å, or 1.0–1.2 Å, from the corresponding positions in the rTS and CeTS, or hTS, complexes, respectively.

Some conformational differences, although smaller in terms of RMSD, can also be observed within the active site. One such difference concerns the position of dUMP and, in turn, distances from the pyrimidine ring to the catalytic Cys197. In subunit A of the mTS–dUMP–Raltitrexed complex, which, from among the analyzed structures, populates the most closed state of the active site pocket, the uracil moiety of dUMP is much closer to the catalytic cysteine (C6 of dUMP-γS of Cys197 distance of 2.5 Å), compared to the corresponding structures of rat, human and *C. elegans* TSs (C6-γS distances of 3.5, 3.4 and 3.4 Å, respectively). This positional change of dUMP is accompanied by changes in the positions of selected amino acid residues involved in dUMP binding (Arg177′, Arg178′, Arg51, Arg217, His258 and Tyr260), placed differently in mTS, compared to rTS, hTS and *Ce*TS complexes. Another difference concerns *Ce*TS His198 (His190 in rTS and mTS and His196 in hTS). Like in the binary complexes, the position of His198 is different in the ternary complexes of the mammalian enzymes, where the imidazole side chain of His198 participates in a water-mediated hydrogen bond network stabilizing the position of dUMP O4, compared to the ternary complex of nematode TS, where the His198 side chain is rotated away from the uracil moiety of dUMP and towards the side chain of Tyr232, with the His198-Tyr232 H-bond formation sealing the displacement of His198 (Fig. 7). The latter difference does not seem critical for catalysis, but may likely be a factor involved in a discrimination of C4-substituted uracil analogues. In accord, inhibition of purified *T. spiralis* and rat thymidylate synthases by N4-hydroxy-dCMP showed a feeble selectivity towards the parasitic nematode enzyme [16].

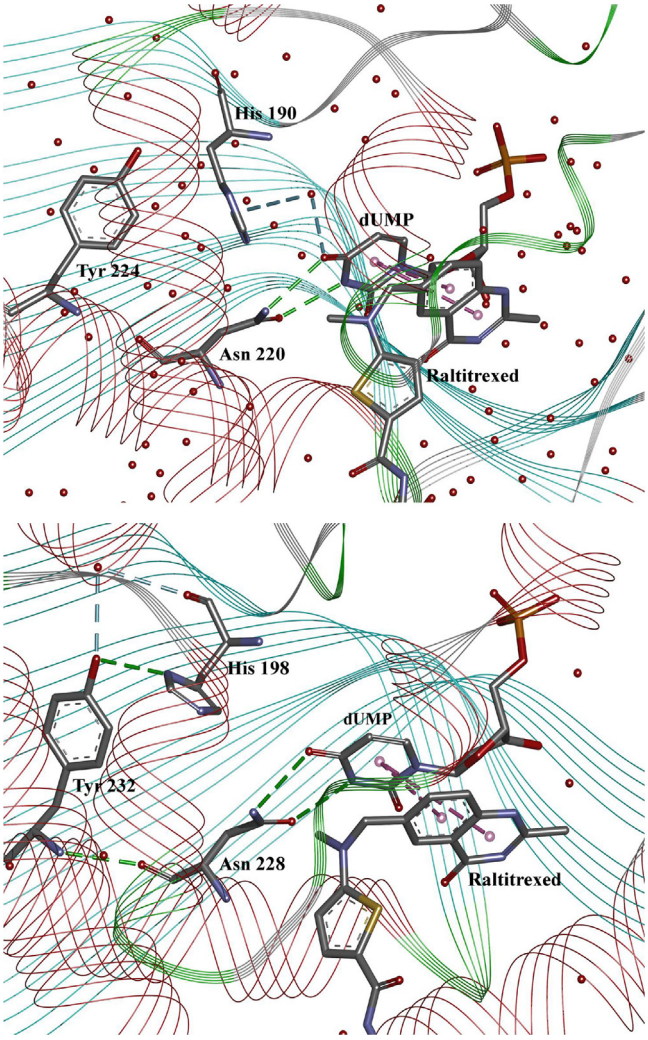

Fig. 7. Different arrangements of His190 in mTS-dUMP-Raltitrexed [top] and equivalent His198 in *Ce*TS-dUMP-Raltitrexed [bottom]. Hydrogen bonds and hydrophobic contacts are shown as dashed lines.

The second ligand in the ternary complexes, Raltitrexed, is located similarly in both the CeTS structure and all structures of mammalian TSs (hTS, mTS and rTS). Most of its interactions with protein residues and dUMP, either hydrophobic or electrostatic (including H-bonding), are preserved in all compared structures. And even though some interactions of Raltitrexed are not shared among all ternary complexes, none of them pertains exclusively to the nematode enzyme.

3.8. Comparison of the structural ensembles generated with tCONCOORD

The Cα RMSF profiles of the structural ensembles generated with tCONCOORD are shown in Figs. 2C, 4C, 5C and 6C. Overall, all the RMSF profiles, regardless if for subunit A or B, are mutu-

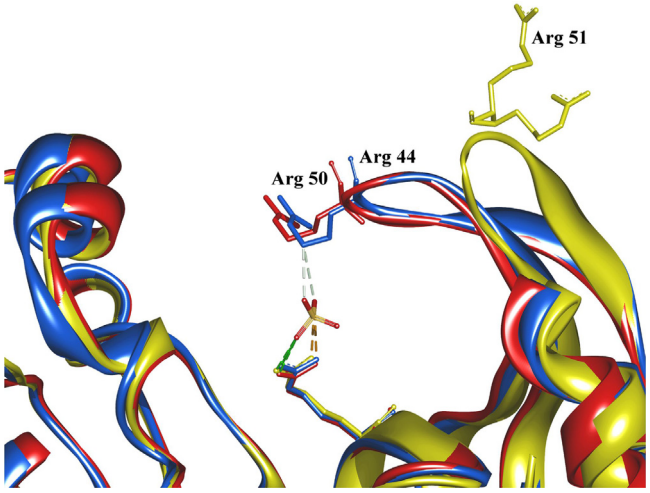

Fig. 8. Different arrangements of Arg 51 in *Ce*TS (yellow) and equivalent Arg 50 and Arg 44 in hTS (blue) and mTS (red), respectively. Hydrogen bonds are shown as dashed lines. (For interpretation of the references to colour in this figure legend, the reader is referred to the web version of this article.)

ally similar, with consistent maxima and minima positions. The largest peaks describe the fluctuations of mobile segments on or near the surface of the protein: (i) the active site flanking segment, AA5 helix-loop Ser114-Gly129, (ii) the large segment starting at the C-terminal Thr306, extending through long circular loops and the AB4-AB1 helices to a few residues in an outer shell surrounding the active site, including Tyr258, (iii) the Ala144-Gln156 loop located in the proximity of the AA6 and AA7 helices, (iv) the active site AA8 helix-loop region Asp186-Pro193, (v) the active site-adjacent loop-AA3 helix region Ser95-Gly105, (vi) the loop fragment Leu74-Arg78 preceding the central AA2 helix 80–94, and (vii) the segment 68–70 in a loop nearby the second strand of the central β-sheet (all numbering according to the hTS sequence). On the other hand, the dimerization interface region is weakly flexible in both mammalian and nematode enzymes.

Despite the "positional" similarity of the profiles, there are differences in the height of the peaks, as well as in the overall flexibilities, between the two nematode enzymes (*Ce*TS vs. *Ts*TS) and between each of them and the mammalian (hTS, mTS and rTS) enzymes. The *Ts*TS enzyme is less flexible than the mouse enzyme but more flexible than the *Ce*TS enzyme. The latter enzyme appears to be the least flexible, and the peaks in its B-factor profile lower, compared to the mammalian and *Ts*TS enzymes.

A single local region, showing larger flexibility on the part of the *Ce*TS enzyme, is the active site flanking loop Lys47-Gly54, wherein a sharp peak for the ligand-free *Ce*TS strongly surpasses much smaller peaks for the ligand-free hTS and mTS (Fig. 2C). In the ligand-free *Ce*TS, the side chain of Arg51 is too far from the AS sulfate anion and does not form a hydrogen bond with it (Fig. 8). Due to this and its location on the protein surface, the *Ce*TS Arg51 turns out to be a very flexible residue, which in the crystal structure of *Ce*TS is populating two alternative conformations. The corresponding arginine residues in the ligand-free hTS and mTS structures are either hydrogen bonded, or at least strongly electrostatically attracted, to "their" sulfate anions and therefore much less flexible. This difference concerns only the ligand-free, but not ligand-bound, enzymes. Apart from it, there are no other distinct RMSF differences between these two groups of enzymes.

3.9. Molecular docking to nematode (*Ts*TS) vs. mammalian (hTS) receptors

The selected results for binding affinities, calculated as docking scores and binding free energies, are presented in Table 4. For convenience, docking scores are reported as logarithms of averages from computed HYDE affinity ranges. Values smaller than 3 or higher than 5 indicate very high or low ligand-receptor affinities, respectively. Decomposition of the computed binding free energies on a per-residue basis is shown as Supplementary Material.

One group of ligands, the derivatives of E63 (IUPAC name: 1-({[2-(1-methyl-3-pyrrolidinyl)-1H-imidazol-4-yl]methyl}amino)-2-(5-methyl-2-Thienyl)-1-ethanone), has emerged as possible selective inhibitors of nematode TS based on both their binding affinities and, no less importantly, their interactions with non-conserved residues of *T. spiralis* TS. The group can be defined as coherent in terms of high global similarity to parent compound E63, with the global similarity scores calculated in FTrees [119] between E63 and E63.1, E63.2, E63.3, and E63.4 being, respectively, 0.987, 0.846, 0.670, and 0.846, as well as of the presence of the same structural motifs (e.g. imidazole ring or N-methylformamide moiety). Detailed comparison of E63 and its chosen derivatives is presented as Supplementary Material. The docking scores and binding free energies in this group favor several *Ts*TS complexes over corresponding hTS complexes (Table 4). The decompositions of the binding free energies point to several differences in the receptor-ligand interactions in the *Ts*TS compared to hTS complexes (exemplary binding poses are shown in Figs. 9 and 10; 2D interaction diagrams prepared using Ligand Interactions tool from Discovery Studio 4.5 Visualizer are available as Supplementary Material). In particular, in the former complexes some strictly specific interactions with certain non-conserved residues in the dimerization interface can be observed, including (i) hydrogen bonds with Thr174 from at least one subunit (all compounds from the E63 family), (ii) hydrophobic π-alkyl interaction with Phe192 from subunit A (E63.2), (iii) hydrophobic interactions with Cys191 from either subunit A (π-sulfur interaction with E63.3) or subunit B (alkyl interaction with E63.2), and (iv) hydrophobic interactions with Tyr152 from subunit A (π-sulfur interaction with E63.1 or π-alkyl interaction with E63.3). Among ligands in this group, interactions with *Ts*TS are more persistent than with hTS, especially considering the difference between highly populated and strongly contributing to binding H-bonds with Thr174 from *Ts*TS and lowly populated and weakly contributing to binding hydrophobic interactions with equivalent Cys180 from hTS (the latter interactions present for E63 (subunit B) and E63.4 (both subunits)). Other non-conserved hTS residues engage only very little (Val158) or not at all (Leu198 and Ala197) in interactions corresponding to those observed for *Ts*TS Tyr152, Phe192 and Cys191, respectively. Moreover, some of the ligands from the E63 family (E63.1, E63.2, E63.3) do not exhibit any interactions with the non-conserved residues of hTS. As well, the consistent, central structural motif of the E63 family does not participate in conventional hydrogen bonding with the hTS receptor in case of both E63 and the two derivatives, E63.2 and E63.4, underlining the selective nature of presented interactions. Additionally, several interactions with conserved residues also contribute to stable binding of the E63 derivatives to *Ts*TS throughout the MD simulations (compare energy decomposition diagrams in Supplementary Material).

The E63 family of ligands may thus be considered as either structural lead for nematode TS-specific drug design by itself, or at least a mean of bringing attention to a region of the enzyme that exhibits potentially prominent variability between the human and nematode TSs.

Table 4
Binding affinities of selected ligands for *Ts*TS and hTS. Docking scores provided as logarithms of average HYDE affinities are compared with binding free energies computed using MM-GBSA method on 10 ns AMBER MD trajectories.

Ligand symbol and structure	Affinity vs *Ts*TS		Affinity vs hTS	
	log(average HYDE affinity)	Free energy of binding [kcal/mol]	log(average HYDE affinity)	Free energy of binding [kcal/mol]
E63 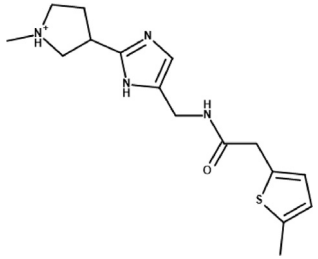	1.00	−32.06	4.36	−20.32
E63.1 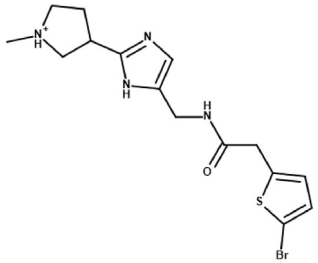	1.08	−39.90	4.90	−22.81
E63.2 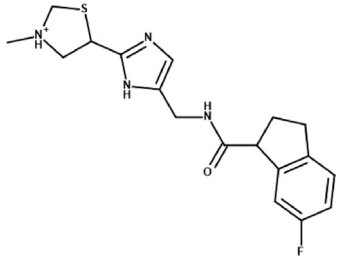	0.19	−30.82	4.92	−19.10
E63.3 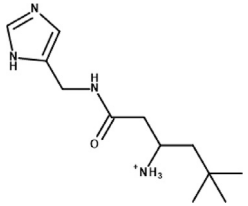	2.28	−25.99	5.70	−14.68
E63.4 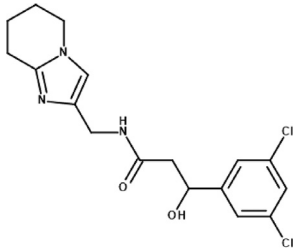	2.74	−40.68	5.01	−29.17

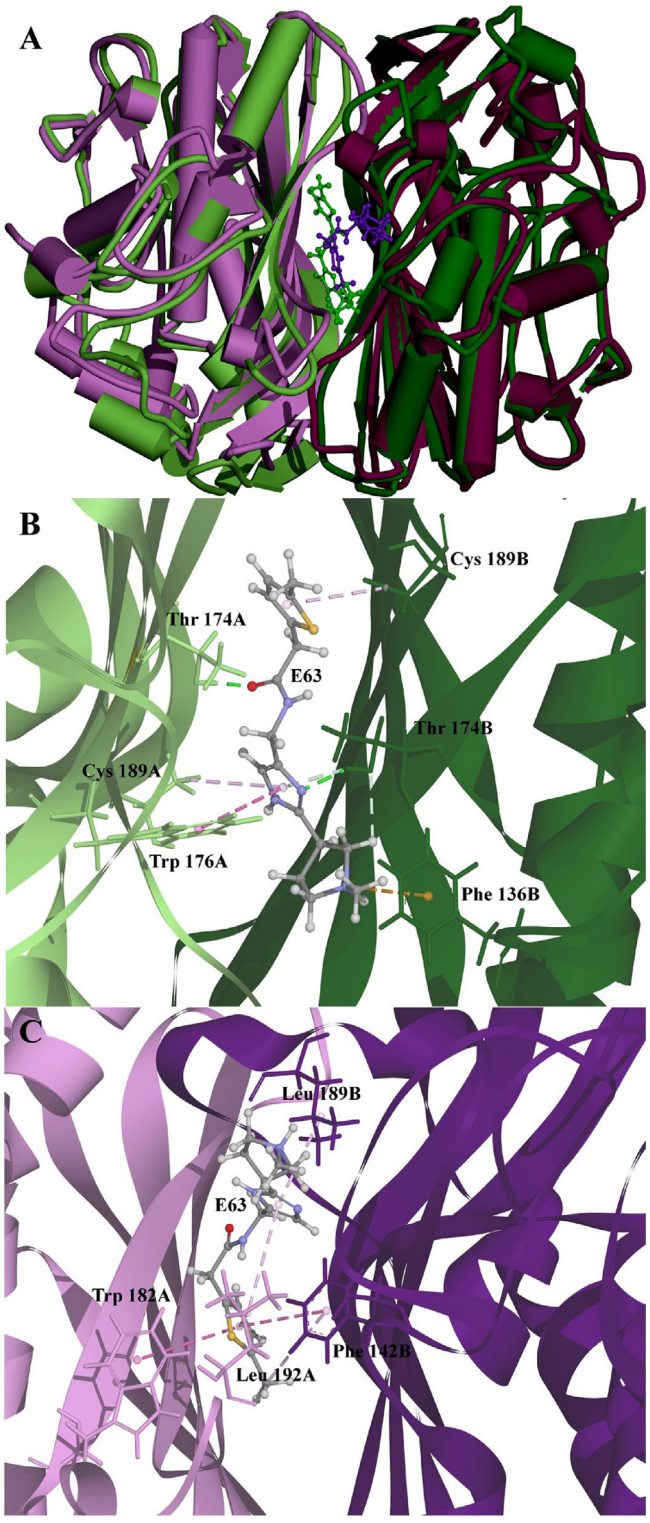

Fig. 9. Binding of E63 to the dimerization interfaces of *Ts*TS and hTS. [A] Binding position of E63 in the complete dimers of *Ts*TS (green) and hTS (violet). [B] The binding site of E63 in the dimerization interface of *Ts*TS. [C] The binding site of E63 in the dimerization interface of hTS. Residues engaged in non-bonded interactions with E63 are shown as sticks. Interactions are shown as dashed lines. Subunits A and B are shown light green and green, respectively, in *Ts*TS, or light violet and violet, respectively, in hTS. (For interpretation of the references to colour in this figure legend, the reader is referred to the web version of this article.)

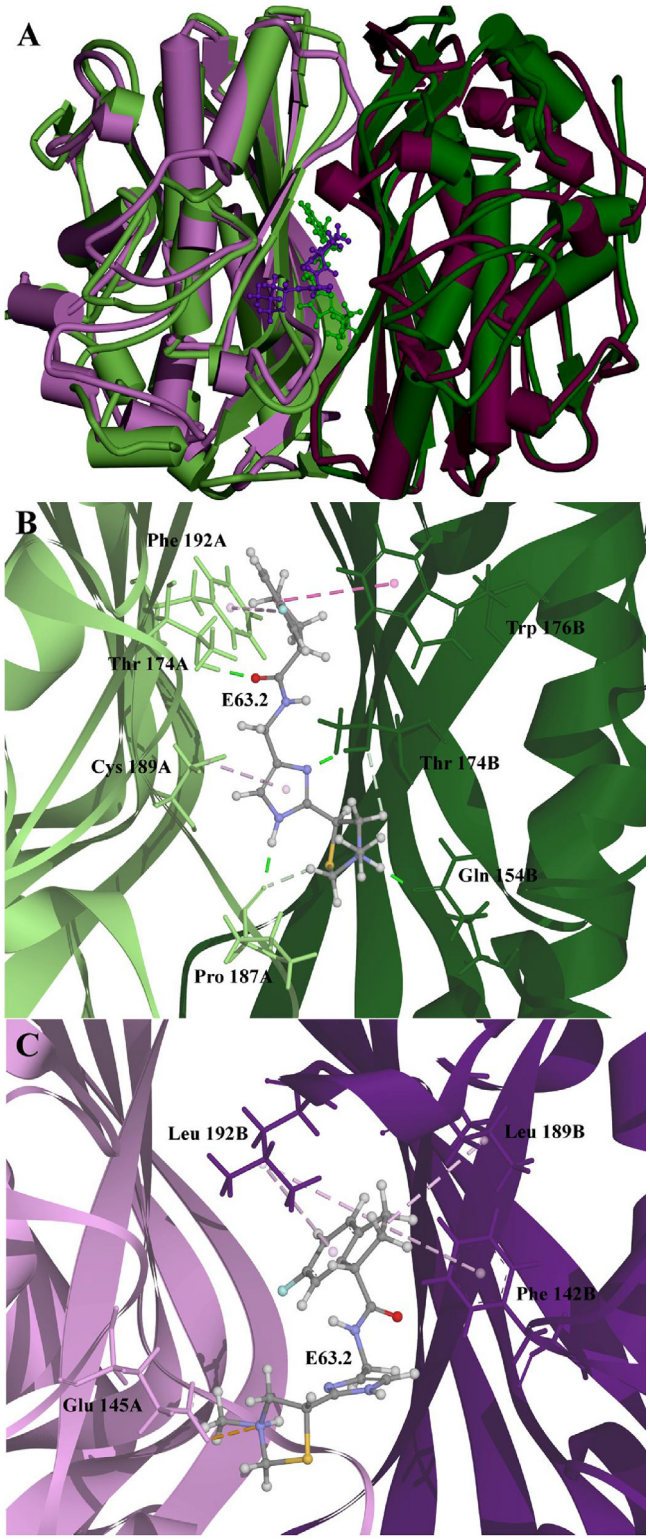

Fig. 10. Binding of E63.2 to the dimerization interfaces of *Ts*TS and hTS. [A] Binding position of E63.2 in the complete dimers of *Ts*TS (green) and hTS (violet). [B] The binding site of E63.2 in the dimerization interface of *Ts*TS. [C] The binding site of E63.2 in the dimerization interface of hTS. Residues engaged in non-bonded interactions with E63.2 are shown as sticks. Interactions are shown as dashed lines. Subunits A and B are shown light green and green, respectively, in *Ts*TS, or light violet and violet, respectively, in hTS. (For interpretation of the references to colour in this figure legend, the reader is referred to the web version of this article.)

4. Conclusions

In search of a template for the species-specific drug design, comparative analysis of structure and basic dynamics across the ligand-free and ligand-bound nematode and mammalian thymidylate synthases was made. Furthermore, comparative molecular docking complemented with molecular dynamics and trajectories' post-analysis, including free energy of binding computations, were performed in search of ligands showing potential of selective inhibition of *T. spiralis* TS. Overall, the structures of mammalian and nematode thymidylate synthases, as well as their dynamic behaviors, are strongly mutually similar. In spite of it, the results of molecular docking pointed out to a pool of compounds, the E63 family, exerting predictively a strong and selective binding to *Ts*TS. This prediction is based on both favorable docking scores and binding free energies, as well as the occurrences of several species-specific interactions with residues located in the dimerization interface of *Ts*TS (including Thr174, Phe192, Cys191 and Tyr152). The E63 family of ligands is worth of experimental validation and, even regardless of the direct outcome, seems promising for further optimization towards development of selective allosteric inhibitors of *Ts*TS and future agents against trichinellosis.

Acknowledgments

Supported by the Ministry of Science and Higher Education (Grant No. N301 3948 33) and by the National Science Centre (grants Nos. 2011/01/B/NZ6/01781 and 2015/18/E/NZ1/00689).

Authors are grateful for access to the X-ray generator at the core facilities of the International Institute of Molecular and Cell Biology in Warsaw, Poland, and to Dr. Roman Szczepanowski for help in data collection.

The Helmholtz Zentrum Berlin is acknowledged for allocation of synchrotron radiation beamtime, its use being supported by the European Community's Seventh Framework Programme (FP7/2007-2013) under BioStruct-X (grant agreement No. 283570).

License for LeadIT, SeeSAR, and FTrees was awarded in the BioSolveIT Summer Challenge 2016 organized by BioSolveIT GmbH.

The calculations mentioned in this paper were partly performed using the PLATON project's infrastructure at the Technical University of Lodz Computer Centre.

References

[1] P. Pacifico, Nematodes: worms of the world, MLO Med. Lab. Obs. 33 (2001) 24–31.
[2] P.J. Hotez, P.J. Brindley, J.M. Bethony, C.H. King, E.J. Pearce, J. Jacobson, Helminth infections: the great neglected tropical diseases, J. Clin. Invest. 118 (2008) 1311–1321.
[3] C. L'Ollivier, R. Piarroux, Diagnosis of human nematode infections, Expert Rev. Anti. Infect. Ther. 11 (2013) 1363–1376.
[4] K.D. Murrell, E. Pozio, Trichinellosis: the zoonosis that won't go quietly, Int. J. Parasitol. 30 (2000) 1339–1349.
[5] K.D. Murrell, E. Pozio, Worldwide occurrence and impact of human trichinellosis, 1986–2009, Emerg. Infect. Dis. 17 (2011) 2194–2202.
[6] T.R. Bürglin, E. Labos, M.L. Blaxter, Caenorhabditis elegans as a model for parasitic nematodes, Int. J. Parasitol. 28 (1998) 395–411.
[7] A.R. Burns, G.M. Luciani, G. Musso, R. Bagg, M. Yeo, Y. Zhang, L. Rajendran, J. Glavin, R. Hunter, E. Redman, S. Stasiuk, M. Schertzberg, G.A. McQuibban, C.R. Caffrey, S.R. Cutler, M. Tyers, G. Giaever, C. Nislow, A.G. Fraser, C.A. MacRae, J. Gilleard, P.J. Roy, Caenorhabditis elegans is a useful model for anthelmintic discovery, Nat. Commun. 6 (2015) 7485.
[8] P. Chaweeborisuit, C. Suriyonplengsaeng, W. Suphamungmee, P. Sobhon, K. Meemon, Nematicidal effect of plumbagin on Caenorhabditis elegans: a model for testing a nematicidal drug, Z. Naturforsch. C 71 (2016) 121–131.
[9] N.H. Georgopapadakou, T.J. Walsh, Antifungal agents: chemotherapeutic targets and immunologic strategies, Antimicrob. Agents Chemother. 40 (1996) 279–291.
[10] P.K. Rathod, Antimalarial agents directed at thymidylate synthase, J. Pharm. Pharmacol. 49 (2) (1997) 704–711.
[11] Y. Takemura, A.L. Jackman, Folate-based thymidylate synthase inhibitors in cancer chemotherapy, Anticancer Drugs 8 (1997) 3–16.
[12] M.P. Costi, S. Ferrari, A. Venturelli, S. Calo, D. Tondi, D. Barlocco, Thymidylate synthase structure, function and implication in drug discovery, Curr. Med. Chem. 12 (2005) 2241–2258.
[13] W.H. Gmeiner, Novel chemical strategies for thymidylate synthase inhibition, Curr. Med. Chem. 12 (2005) 191–202.
[14] P. Singh, A. Bhardwaj, Mechanism of action of key enzymes associated with cancer propagation and their inhibition by various chemotherapeutic agents, Mini Rev. Med. Chem. 8 (2008) 388–398.
[15] A. Jarmuła, Antifolate inhibitors of thymidylate synthase as anticancer drugs, Mini Rev. Med. Chem. 10 (2010) 1211–1222.
[16] W. Rode, M. Dąbrowska, Z. Zieliński, B. Gołos, M. Wranicz, K. Felczak, T. Kulikowski, Trichinella spiralis and Trichinella pseudospiralis: developmental patterns of enzymes involved in thymidylate biosynthesis and pyrimidine salvage, Parasitology 120 (2000) 593–600.
[17] M. Dąbrowska, E. Jagielska, J. Cieśla, A. Płucienniczak, J. Kwiatowski, M. Wranicz, P. Boireau, W. Rode, *Trichinella spiralis* thymidylate synthase: cDNA cloning and sequencing, and developmental pattern of mRNA expression, Parasitology 128 (2004) 209–221.
[18] P. Wińska, B. Gołos, J. Cieśla, Z. Zieliński, T. Frączyk, E. Wałajtys-Rode, W. Rode, Developmental arrest in Caenorhabditis elegans dauer larvae causes high expression of enzymes involved in thymidylate biosynthesis, similar to that found in Trichinella muscle larvae, Parasitology 131 (2005) 247–254.
[19] B. Gołos, M. Dąbrowska, E. Wałajtys-Rode, Z. Zieliński, P. Wińska, J. Cieśla, E. Jagielska, T. Moczoń, W. Rode, Immunofluorescent localization of thymidylate synthase in the development of Trichinella spiralis and Caenorhabditis elegans, Mol. Biochem. Parasitol. 183 (2012) 63–69.
[20] E. Jagielska, A. Płucienniczak, M. Dąbrowska, A. Dowierciał, W. Rode, Trichinella pseudospiralis vs. T. spiralis thymidylate synthase gene structure and T. pseudospiralis thymidylate synthase retrogene sequence, Parasit. Vectors 7 (2014) 175.
[21] L.A. Parsels, E. Chu, The role of translational control of the cell cycle, Cancer J. 4 (1998) 287–295.
[22] L. Rahman, D. Voeller, M. Rahman, S. Lipkowitz, C. Allegra, J.C. Barrett, F.J. Kaye, M. Zajac-Kaye, Thymidylate synthase as an oncogene: a novel role for an essential DNA synthesis enzyme, Cancer Cell 5 (2004) 341–351.
[23] K.M. Perry, E.B. Fauman, J.S. Finer-Moore, W.R. Montfort, G.F. Maley, F. Maley, R.M. Stroud, Plastic adaptation toward mutations in proteins: structural comparison of thymidylate synthases, Proteins 8 (1990) 315–333.
[24] C.W. Carreras, D.V. Santi, The catalytic mechanism and structure of thymidylate synthase, Annu. Rev. Biochem. 64 (1995) 721–762.
[25] R.M. Stroud, J.S. Finer-Moore, Conformational dynamics along an enzymatic reaction pathway: thymidylate synthase, 'the Movie', Biochemistry 42 (2003) 239–247.
[26] D. Garg, S. Skouloubris, J. Briffotaux, H. Myllykallio, R.C. Wade, Conservation and role of electrostatics in thymidylate synthase, Sci. Rep. 5 (2015) 17356.
[27] B.K. Shoichet, R.M. Stroud, D.V. Santi, I.D. Kuntz, K.M. Perry, Structure-based discovery of inhibitors of thymidylate synthase, Science 259 (1993) 1445–1450.
[28] T.J. Stout, D. Tondi, M. Rinaldi, D. Barlocco, P. Pecorari, D.V. Santi, I.D. Kuntz, R.M. Stroud, B.K. Shoichet, M.P. Costi, Structure-based design of inhibitors specific for bacterial thymidylate synthase, Biochemistry 38 (1999) 1607–1617.
[29] D. Tondi, U. Slomczynska, M.P. Costi, D.M. Watterson, S. Ghelli, B.K. Shoichet, Structure-based discovery and in-parallel optimization of novel competitive inhibitors of thymidylate synthase, Chem. Biol. 6 (1999) 319–331.
[30] T.A. Fritz, D. Tondi, J.S. Finer-Moore, M.P. Costi, R.M. Stroud, Predicting and harnessing protein flexibility in the design of species-specific inhibitors of thymidylate synthase, Chem. Biol. 8 (2001) 981–995.
[31] M.P. Costi, D. Tondi, M. Rinaldi, D. Barlocco, P. Pecorari, F. Soragni, A. Venturelli, R.M. Stroud, Structure-based studies on species-specific inhibition of thymidylate synthase, Biochim. Biophys. Acta 1587 (2002) 206–214.
[32] S. Ferrari, M.P. Costi, R.C. Wade, Inhibitor specificity via protein dynamics: insights from the design of antibacterial agents targeted against thymidylate synthase, Chem. Biol. 10 (2003) 1183–1193.
[33] S. Ghelli, M. Rinaldi, D. Barlocco, A. Gelain, P. Pecorari, D. Tondi, G. Rastelli, M.P. Costi, Ortho-halogen naphthaleins as specific inhibitors of Lactobacillus casei thymidylate synthase: conformational properties and biological activity, Bioorg. Med. Chem. 11 (2003) 951–963.
[34] D. Tondi, A. Venturelli, S. Ferrari, S. Ghelli, M.P. Costi, Improving specificity vs bacterial thymidylate synthases through N-dansyl modulation of didansyltyrosine, J. Med. Chem. 48 (2005) 913–916.
[35] J.S. Finer-Moore, A.C. Anderson, R.H. O'Neil, M.P. Costi, S. Ferrari, J. Krucinski, R.M. Stroud, The structure of *Cryptococcus neoformans* thymidylate synthase suggests strategies for using target dynamics for species-specific inhibition, Acta Crystallogr. D Biol. Crystallogr. 61 (2005) 1320–1334.
[36] M.P. Costi, A. Gelain, D. Barlocco, S. Ghelli, F. Soragni, F. Reniero, T. Rossi, A. Ruberto, C. Guillou, A. Cavazzuti, C. Casolari, S. Ferrari, Antibacterial agent discovery using thymidylate synthase biolibrary screening, J. Med. Chem. 49 (2006) 5958–5968.
[37] S. Ferrari, V. Losasso, M.P. Costi, Sequence-based identification of specific drug target regions in the thymidylate synthase enzyme family, ChemMedChem 3 (2008) 392–401.
[38] S. Calo, D. Tondi, S. Ferrari, A. Venturelli, S. Ghelli, M.P. Costi, Constrained dansyl derivatives reveal bacterial specificity of highly conserved thymidylate synthases, Chembiochem 9 (2008) 779–790.

[39] S. Mangani, L. Cancian, R. Leone, C. Pozzi, S. Lazzari, R. Luciani, S. Ferrari, M.P. Costi, Identification of the binding modes of N-phenylphthalimides inhibiting bacterial thymidylate synthase through X-ray crystallography screening, J. Med. Chem. 54 (2011) 5454–5467.
[40] S. Ferrari, M. Ingrami, F. Soragni, R.C. Wade, M.P. Costi, Ligand-based discovery of N-(1,3-dioxo-1H,3H-benzo[de]isochromen-5-yl)-carboxamide and sulfonamide derivatives as thymidylate synthase A inhibitors, Bioorg. Med. Chem. Lett. 23 (2013) 663–668.
[41] S. Ferrari, S. Calò, R. Leone, R. Luciani, L. Costantino, S. Sammak, F. Di Pisa, C. Pozzi, S. Mangani, M.P. Costi, 2'-Deoxyuridine 5'-monophosphate substrate displacement in thymidylate synthase through 6-hydroxy-2H-naphtho[1,8-bc]furan-2-one derivatives, J. Med. Chem. 56 (2013) 9356–9360.
[42] J. Phan, S. Koli, W. Minor, R.B. Dunlap, S.H. Berger, L. Lebioda, Human thymidylate synthase is in the closed conformation when complexed with dUMP and raltitrexed, an antifolate drug, Biochemistry 40 (2001) 1897–1902.
[43] J. Phan, D.J. Steadman, S. Koli, W.C. Ding, W. Minor, R.B. Dunlap, S.H. Berger, L. Lebioda, Structure of human thymidylate synthase suggests advantages of chemotherapy with noncompetitive inhibitors, J. Biol. Chem. 276 (2001) 14170–14177.
[44] R. Almog, C.A. Wadlling, F. Maley, G.F. Maley, P. Van Roey, Crystal structure of a deletion mutant of human thymidylate synthase Δ (7–29) and its ternary complex with Tomudex and dUMP, Protein Sci. 10 (2001) 988–996.
[45] P.H. Sayre, J.S. Finer-Moore, T.A. Fritz, D. Biermann, S.B. Gates, W.C. MacKellar, V.F. Patel, R.M. Stroud, Multi-targeted antifolates aimed at avoiding drug resistance form covalent closed inhibitory complexes with human and Escherichia coli thymidylate synthases, J. Mol. Biol. 313 (2001) 813–829.
[46] L.L. Lovelace, W. Minor, L. Lebioda, Structure of human thymidylate synthase under low-salt conditions, Acta Crystallogr. D Biol. Crystallogr. 61 (2005) 622–627.
[47] L.L. Lovelace, L.M. Gibson, L. Lebioda, Cooperative inhibition of human thymidylate synthase by mixtures of active site binding and allosteric inhibitors, Biochemistry 46 (2007) 2823–2830.
[48] L.M. Gibson, L.L. Lovelace, L. Lebioda, The R163 K mutant of human thymidylate synthase is stabilized in an active conformation: structural asymmetry and reactivity of cysteine 195, Biochemistry 47 (2008) 4636–4643.
[49] L.L. Lovelace, S.R. Johnson, L.M. Gibson, B.J. Bell, S.H. Berger, L. Lebioda, Variants of human thymidylate synthase with loop 181–197 stabilized in the inactive conformation, Protein Sci. 18 (2009) 1628–1636.
[50] X. Huang, L.M. Gibson, B.J. Bell, L.L. Lovelace, M.M. Peña, F.G. Berger, S.H. Berger, L. Lebioda, Replacement of Val3 in human thymidylate synthase affects its kinetic properties and intracellular stability, Biochemistry 49 (2010) 2475–2482.
[51] D. Cardinale, G. Guaitoli, D. Tondi, R. Luciani, S. Henrich, O.M. Salo-Ahen, S. Ferrari, G. Marverti, D. Guerrieri, A. Ligabue, C. Frassineti, C. Pozzi, S. Mangani, D. Fessas, R. Guerrini, G. Ponterini, R.C. Wade, M.P. Costi, Protein-protein interface-binding peptides inhibit the cancer therapy target human thymidylate synthase, Proc. Natl. Acad. Sci. U. S. A. 108 (2011) E542–549.
[52] L.M. Gibson, L.R. Celeste, L.L. Lovelace, L. Lebioda, Structures of human thymidylate synthase R163K with dUMP, FdUMP and glutathione show asymmetric ligand binding, Acta Crystallogr. D Biol. Crystallogr. 67 (2011) 60–66.
[53] R.R. Sotelo-Mundo, J. Cieśla, J.M. Dzik, W. Rode, F. Maley, G.F. Maley, L.W. Hardy, W.R. Montfort, Thymidylate synthase from rat in ternary complex with dUMP and Tomudex, Biochemistry 38 (1999) 1087–1094.
[54] A. Dowiercіał, P. Wilk, W. Rypniewski, W. Rode, A. Jarmuła, Crystal structure of mouse thymidylate synthase in tertiary complex with dUMP and Raltitrexed reveals N-terminus architecture and two different active site conformations, Biomed. Res. Int. (2014), Article ID 945803, 7 pages.
[55] L. Taddia, D. D'Arca, S. Ferrari, C. Marraccini, L. Severi, G. Ponterini, Y.G. Assaraf, G. Marverti, M.P. Costi, Inside the biochemical pathways of thymidylate synthase perturbed by anticancer drugs: novel strategies to overcome cancer chemoresistance, Drug Resist. Updat. 23 (2015) 20–54.
[56] V. Prasanna, S. Bhattacharjya, P. Balaram, Synthetic interface peptides as inactivators of multimeric enzymes: inhibitory and conformational properties of three fragments from Lactobacillus casei thymidylate synthase, Biochemistry 37 (1998) 6883–6893.
[57] G. Cannazza, A.S. Cazzato, C. Marraccini, G. Pavesi, S. Pirondi, R. Guerrini, M. Pelà, C. Frassineti, S. Ferrari, G. Marverti, G. Ponterini, M.P. Costi, Internalization and stability of a thymidylate synthase peptide inhibitor in ovarian cancer cells, J. Med. Chem. 57 (2014) 10551–10556.
[58] M. Pela, P. Saxena, R. Luciani, M. Santucci, S. Ferrari, G. Marverti, C. Marraccini, A. Mortello, S. Pirondi, F. Genovese, S. Salvadori, D. D'Arca, G. Ponterini, M.P. Costi, R. Guerrini, Optimization of peptides that target human thymidylate synthase to inhibit ovarian cancer cell growth, J. Med. Chem. 57 (2014) 1355–1367.
[59] F. Sacchetti, C. Marraccini, D. D'Arca, M. Pela, D. Pinetti, E. Maretti, M. Hanuskova, V. Iannuccelli, M.P. Costi, E. Leo, Enhanced anti-hyperproliferative activity of human thymidylate synthase inhibitor peptide by solid lipid nanoparticle delivery, Colloids Surf. B Biointerfaces 136 (2015) 346–354.
[60] G. Ponterini, A. Martello, G. Pavesi, A. Lauriola, R. Luciani, M. Santucci, M. Pelà, G. Gozzi, S. Pacifico, R. Guerrini, G. Marverti, M.P. Costi, D. D'Arca, Intracellular quantitative detection of human thymidylate synthase engagement with an unconventional inhibitor using tetracysteine-diarsenical-probe technology, Sci. Rep. 6 (2016) 27198.
[61] F. Sacchetti, D. D'Arca, F. Genovese, S. Pacifico, E. Maretti, M. Hanuskova, V. Iannuccelli, M.P. Costi, E. Leo, Conveying a newly designed hydrophilic anti-human thymidylate synthase peptide to cisplatin resistant cancer cells: are pH-sensitive liposomes more effective than conventional ones? Drug Dev. Ind. Pharm. 43 (2017) 465–473.
[62] M.J. Landau, H. Sharma, K.S. Anderson, Selective peptide inhibitors of bifunctional thymidylate synthase-dihydrofolate reductase from *Toxoplasma gondii* provide insights into domain–domain communication and allosteric regulation, Protein Sci. 22 (2013) 1161–1173.
[63] H. Sharma, M.J. Landau, T.J. Sullivan, V.P. Kumar, M.K. Dahlgren, W.L. Jorgensen, K.S. Anderson, Virtual screening reveals allosteric inhibitors of the Toxoplasma gondii thymidylate synthase-dihydrofolate reductase, Bioorg. Med. Chem. Lett. 24 (2014) 1232–1235.
[64] J. Ludwiczak, P. Maj, P. Wilk, T. Frączyk, T. Ruman, B. Kierdaszuk, A. Jarmuła, W. Rode, Phosphorylation of thymidylate synthase affects slow-binding inhibition by 5-fluoro-dUMP and N(4)-hydroxy-dCMP, Mol. Biosyst. 12 (2016) 1333–1341.
[65] F. Wolschin, S. Wienkoop, W. Weckwerth, Enrichment of phosphorylated proteins and peptides from complex mixtures using metal oxide/hydroxide affinity chromatography (MOAC), Proteomics 5 (2005) 4389–4397.
[66] J. Cieśla, T. Fraczyk, Z. Zieliński, J. Sikora, W. Rode, Altered mouse leukemia L1210 thymidylate synthase, associated with cell resistance to 5-fluoro-dUrd, is not mutated but rather reflects posttranslational modification, Acta Biochim. Pol. 53 (2006) 189–198.
[67] A. Dowiercіał, P. Wilk, W. Rypniewski, T. Frączyk, A. Jarmuła, K. Banaszak, M. Dąbrowska, J. Cieśla, W. Rode, Crystal structures of thymidylate synthase from nematodes, Trichinella spiralis and Caenorhabditis elegans, as a potential template for species-specific drug design, Pteridines 24 (Special Issue) (2013) 87–91.
[68] U. Mueller, R. Forster, M. Hellmig, F. Huschmann, A. Kastner, P. Malecki, S. Puhringer, M. Rower, K. Sparta, M. Steffien, M. Uhlein, P. Wilk, M.S. Weiss, The macromolecular crystallography beamlines at BESSY II of the Helmholtz-Zentrum Berlin: current status and perspectives, Eur. Phys. J. Plus 130 (2015) 141–150.
[69] Z. Otwinowski, W. Minor, Processing of X-ray diffraction data collected in oscillation mode, Methods Enzymol. 276 (1997) 307–326.
[70] W. Kabsch, Evaluation of single crystal X-ray diffraction data from a position-sensitive detector, J. Appl. Cryst. 21 (1988) 916–924.
[71] A.J. McCoy, R.W. Grosse-Kunstleve, P.D. Adams, M.D. Winn, L.C. Storoni, R.J. Read, Phaser crystallographic software, J. Appl. Cryst. 40 (2007) 658–674.
[72] M.D. Winn, C.C. Ballard, K.D. Cowtan, E.J. Dodson, P. Emsley, P.R. Evans, R.M. Keegan, E.B. Krissinel, A.G.W. Leslie, A. McCoy, S.J. McNicholas, G.N. Murshudov, N.S. Pannu, E.A. Potterton, H.R. Powell, R.J. Read, A. Vagin, K.S. Wilson, Overview of the CCP4 suite and current developments, Acta Cryst D67 (2011) 235–242.
[73] A. Dowiercіał, A. Jarmuła, P. Wilk, W. Rypniewski, B. Kierdaszuk, W. Rode, Crystal structures of complexes of mouse thymidylate synthase crystallized with N^4-OH-dCMP alone or in the presence of $N^{5,10}$-methylenetetrahydrofolate, Pteridines 24 (Special Issue) (2013) 93–98.
[74] G.N. Murshudov, A.A. Vagin, E.J. Dodson, Refinement of macromolecular structures by the maximum-Likelihood method, Acta Cryst. D 53 (1997) 240–255.
[75] P. Emsley, B. Lohkamp, W.G. Scott, K. Cowtan, Features and development of Coot, Acta Cryst. D66 (2010) 486–501.
[76] P.V. Afonine, R.W. Grosse-Kunstleve, N. Echols, J.J. Headd, N.W. Moriarty, M. Mustyakimov, T.C. Terwilliger, A. Urzhumtsev, P.H. Zwart, P.D. Adams, Towards automated crystallographic structure refinement with phenix refine, Acta Crystallogr. D Biol. Crystallogr. 68 (2012) 352–367.
[77] A.A. Vaguine, J. Richelle, S.J. Wodak, SFCHECK: a unified set of procedures for evaluating the quality of macromolecular structure-factor data and their agreement with the atomic model, Acta Cryst. D 55 (1999) 191–205.
[78] A.L. Morris, M.W. MacArthur, E.G. Hutchinson, J.M. Thornton, Stereochemical quality of protein structure coordinates, Proteins 12 (1992) 345–364.
[79] D. Seeliger, J. Haas, D.L. de Groot, Geometry-based sampling of conformational transitions in proteins, Structure 15 (2007) 1482–1492.
[80] D. Seeliger, B.L. de Groot, tCONCOORD-GUI: visually supported conformational sampling of bioactive molecules, J. Comput. Chem. 30 (2009) 1160–1166.
[81] T.F. Smith, M.S. Waterman, Identification of common molecular subsequences, J. Mol. Biol. 147 (1981) 195–197.
[82] W.R. Pearson, Searching protein sequence libraries: comparison of the sensitivity and selectivity of the Smith-Waterman and FASTA algorithms, Genomics 11 (1991) 635–650.
[83] F. Sievers, A. Wilm, D. Dineen, T.J. Gibson, K. Karplus, W. Li, R. Lopez, H. McWilliam, M. Remmert, J. Söding, J.D. Thompson, D.G. Higgins, Fast, scalable generation of high-quality protein multiple sequence alignments using Clustal Omega, Mol. Syst. Biol. 7 (2011) 539.
[84] E. Krissinel, K. Henrick, Inference of macromolecular assemblies from crystalline state, J. Mol. Biol. 372 (2007) 774–797.

[85] E. Krieger, G. Vriend, New ways to boost molecular dynamics simulations, J. Comput. Chem. 36 (2015) 996–1007.
[86] C. Wang, P. Bradley, D. Baker, Protein-protein docking with backbone flexibility, J. Mol. Biol. 373 (2007) 503–519.
[87] A. Leaver-Fay, M. Tyka, S.M. Lewis, O.F. Lange, J. Thompson, R. Jacak, K. Kaufman, P.D. Renfrew, C.A. Smith, W. Sheffler, I.W. Davis, S. Cooper, A. Treuille, D.J. Mandell, F. Richter, Y.E. Ban, S.J. Fleishman, J.E. Corn, D.E. Kim, S. Lyskov, M. Berrondo, S. Mentzer, Z. Popović, J.J. Havranek, J. Karanicolas, R. Das, J. Meiler, T. Kortemme, J.J. Gray, B. Kuhlman, D. Baker, P. Bradley, ROSETTA3: an object-oriented software suite for the simulation and design of macromolecules, Methods Enzymol. 487 (2011) 545–574.
[88] A.S. Konagurthu, J.C. Whisstock, P.J. Stuckey, A.M. Lesk, MUSTANG: a multiple structural alignment algorithm, Proteins 64 (2006) 559–574.
[89] T. Sterling, J.J. Irwin, ZINC15–ligand discovery for everyone, J. Chem. Inf. Model. 55 (2015) 2324–2337.
[90] M. Valli, R.N. dos Santos, L.D. Figueira, C.H. Nakajima, I. Castro-Gamboa, A.D. Andricopulo, V.S. Bolzani, Development of a natural products database from the biodiversity of Brazil, J. Nat. Prod. 76 (2013) 439–444.
[91] C.Y. Chen, TCM Database@Taiwan: the world's largest traditional Chinese medicine database for drug screening in silico, PLoS One 6 (2011) e15939.
[92] M. Hilbig, S. Urbaczek, I. Groth, S. Heuser, M. Rarey, MONA – Interactive manipulation of molecule collections, J. Chemoinform. 5 (2013) 38.
[93] M. Hilbig, M. Rarey, MONA 2: A light cheminformatics platform for interactive compound library processing, J. Chem. Inf. Model. 55 (2015) 2071–2078.
[94] M. Rarey, B. Kramer, T. Lengauer, G. Klebe, A fast flexible docking method using an incremental construction algorithm, J. Mol. Biol. 261 (1996) 470–489.
[95] N. Schneider, S. Hindle, G. Lange, R. Klein, J. Albrecht, H. Briem, K. Beyer, H. Claußen, M. Gastreich, C. Lemmen, M. Rarey, Substantial improvements in large-scale redocking and screening using the novel HYDE scoring function, J. Comput. Aided Mol. Des. 26 (2012) 701–723.
[96] N. Schneider, G. Lange, S. Hindle, R. Klein, M. Rarey, A consistent description of HYdrogen bond and DEhydration energies in protein-ligand complexes: methods behind the HYDE scoring function, J. Comput. Aided Mol. Des. 27 (2013) 15–29.
[97] W.L. Jorgensen, J. Chandrasekhar, J.D. Madura, R.W. Impey, M.L. Klein, Comparison of simple potential functions for simulating liquid water, J. Chem Phys. 79 (1983) 926–935.
[98] D.A. Case, V. Babin, J.T. Berryman, R.M. Betz, Q. Cai, D.S. Cerutti, I.I.I. Cheatham, T.E. Darden, T.A. Duke, R.E. Gohlke, H. Goetz, A.W. Gusarov, S. Homeyer, N. Janowski, P. Kaus, J. Kolossváry, I. Kovalenko, A. Lee, T.S. LeGrand, S. Luchko, T. Luo, R. Madej, B. Merz, K.M. Paesani, F. Roe, D.R. Roitberg, A. Sagui, C. Salomon-Ferrer, R. Seabra, G. Simmerling, C.L. Smith, W. Swails, J. Walker, R.C. Wang, J. Wolf, R.M. Wu, P.A. Kollman, AMBER 14, University of California, San Francisco, 2014.
[99] J.A. Maier, C. Martinez, K. Kasavajhala, L. Wickstrom, K.E. Hauser, C. Simmerling, ff14SB: improving the accuracy of protein side chain and backbone parameters from ff99SB, J. Chem. Theory Comput. 11 (2015) 3696–3713.
[100] J. Wang, R.M. Wolf, J.W. Caldwell, P.A. Kollman, D.A. Case, Development and testing of a general AMBER force field, J. Comput. Chem. 25 (2004) 1157–1174.
[101] A. Jakalian, B.L. Bush, D.B. Jack, C.I. Bayly, Fast, efficient generation of high-quality atomic charges. AM1-BCC model: I. Method, J. Comput. Chem. 21 (2000) 132–146.
[102] A. Jakalian, D.B. Jack, C.I. Bayly, Fast, efficient generation of high-quality atomic charges. AM1-BCC model: II. Parametrization and validation, J. Comput. Chem. 23 (2002) 1623–1641.
[103] R.L. Davidchack, R. Handel, M.V. Tretyakov, Langevin thermostat for rigid body dynamics, J. Chem. Phys. 130 (2009) 234101.
[104] J.P. Ryckaert, G. Ciccotti, H.J.C. Berendsen, Numerical integration of the Cartesian equations of motion of a system with constraints: molecular dynamics of n-Alkanes, J. Comput. Phys. 23 (1977) 327–341.
[105] D.M. York, T.A. Darden, L.G. Pedersen, The effect of long-range electrostatic interactions in simulations of macromolecular crystals: a comparison of the Ewald and truncated list methods, J. Chem. Phys. 99 (1993) 8345–8348.
[106] U. Essmann, L. Perera, M.L. Berkowitz, T. Darden, H. Lee, L.G. Pedersen, A smooth particle mesh Ewald method, J. Chem. Phys. 103 (1995) 8577–8593.
[107] P.A. Kollman, I. Massova, C. Reyes, B. Kuhn, S. Huo, L. Chong, M. Lee, T. Lee, Y. Duan, W. Wang, O. Donini, P. Cieplak, J. Srinivasan, D.A. Case, T.E. Cheatham III, Calculating structures and free energies of complex molecules: combining molecular mechanics and continuum models, Acc. Chem. Res. 33 (2000) 889–897.
[108] S. Genheden, U. Ryde, The MM/PBSA and MM/GBSA methods to estimate ligand-binding affinities, Expert Opin. Drug Discov. 10 (2015) 449–461.
[109] A. Onufriev, D. Bashford, D.A. Case, Exploring protein native states and large-scale conformational changes with a modified generalized Born model, Proteins 55 (2004) 383–394.
[110] J. Weiser, P.S. Shenkin, W.C. Still, Approximate atomic surfaces from linear combinations of pairwise overlaps (LCPO), J. Comput. Chem. 20 (1999) 217–230.
[111] A. Dowierciał, A. Jarmuła, P. Wilk, W. Rypniewski, M. Kowalska, T. Frączyk, J. Cieśla, W. Rode, Mouse thymidylate synthase does not show the inactive conformation, observed for the human enzyme, Struct. Chem. 28 (2017) 667–674.
[112] N.D. Brunn, S.M. Dibrov, M.B. Kao, M. Ghassemian, T. Hermann, Analysis of mRNA recognition by human thymidylate synthase, Biosci. Rep. 34 (2014) (art: e00168).
[113] P. De Ley, A quick tour of nematode diversity and the backbone of nematode phylogeny, WormBook (2006) 1–8, http://dx.doi.org/10.1895/wormbook.1.41.1, Jan 25.
[114] A. Coghlan, Nematode genome evolution, WormBook (2005) 1–15, http://dx.doi.org/10.1895/wormbook.1.15.1, Sep 7.
[115] M. Mitreva, M.L. Blaxter, D.M. Bird, J.P. McCarter, Comparative genomics of nematodes, Trends Genet. 21 (2005) 573–581.
[116] R.J. Sommer, A. Streit, Comparative genetics and genomics of nematodes: genome structure development, and lifestyle, Annu. Rev. Genet. 45 (2011) 1–20.
[117] T.J. Stout, C.R. Sage, R.M. Stroud, The additivity of substrate fragments in enzyme-ligand binding, Structure 6 (1998) 839–848.
[118] E.E. Rutenber, R.M. Stroud, Binding of the anticancer drug ZD1694 to E. coli thymidylate synthase: assessing specificity and affinity, Structure 4 (1996) 1317–1324.
[119] M. Rarey, J.S. Dixon, Feature trees: a new molecular similarity measure based on tree matching, J. Comput. Aided Mol. Des. 12 (1998) 471–490.